Technical Note N-1209

STUDIES IN SATURATED POOL BOILING OF WATER

by

S. C. GARG

January 1972

NAVAL CIVIL ENGINEERING LABORATORY
Port Hueneme, California 93043

STUDIES IN SATURATED POOL BOILING OF WATER

Technical Note N-1209

ZFXX.512.001.004

by

S. C. Garg

ABSTRACT

A photographic study of saturated nucleate pool boiling of water on horizontally mounted wires and tubes was carried out. The effects of the diameter of the heating surface, system pressure and heat flux upon the bubble diameter at departure from the heating surface were investigated. Five platinum wires of diameter between 0.001 and 0.026 inch and two platinum tubes of diameter 0.05 and 0.10 inch were used at pressures between 1.0 and 14.7 psia. Departure diameter of more than 1,800 discrete bubbles was measured at heat fluxes up to 125,000 Btu/hr-ft^2 by a frame by frame analysis of 6,100 feet of 16 mm film taken at 3,000 and 5,000 frames per second.

The bubble diameter data were compared with analytical expressions by Owens, Ivey and Morris and Garg. An empirical expression is proposed which successfully correlates the bubble diameters in saturated nucleate pool boiling of water at all pressures. Recommendations are made to systematically investigate the effects of surface roughness and the degree of subcooling upon the bubble diameters at departure in nucleate pool boiling.

Approved for public release; distribution unlimited.

Unclassified

Security Classification

DOCUMENT CONTROL DATA - R & D

Security classification of title, body of abstract and indexing annotation must be ente ' when the overall report is classified)

1 ORIGINATING ACTIVITY (Corporate author) Naval Civil Engineering Laboratory Port Hueneme, California 93043	2a. REPORT SECURITY CLASSIFICATION Unclassified 2b. GROUP

3 REPORT TITLE

STUDIES IN SATURATED POOL BOILING OF WATER

4 DESCRIPTIVE NOTES (Type of report and inclusive dates)

5 AUTHOR(S) (First name, middle initial, last name)

S. C. Garg, Ph.D.

6 REPORT DATE	7a. TOTAL NO OF PAGES	7b. NO OF REFS
January 1972	58	16

8a CONTRACT OR GRANT NO	9a ORIGINATOR'S REPORT NUMBER(S)
b. PROJECT NO ZFXX-512-001-004	N-1209
c.	9b. OTHER REPORT NO(S) (Any other numbers that may be assigned this report)
d.	

10 DISTRIBUTION STATEMENT

Approved for public release; distribution unlimited.

11 SUPPLEMENTARY NOTES	12 SPONSORING MILITARY ACTIVITY
	Director of Navy Laboratories

13 ABSTRACT

A photographic study of saturated nucleate pool boiling of water on horizontally mounted wires and tubes was carried out. The effects of the diameter of the heating surface, system pressure and heat flux upon the bubble diameter at departure from the heating surface were investigated. Five platinum wires of diameter between 0.001 and 0.026 inch and two platinum tubes of diameter 0.05 and 0.10 inch were used at pressures between 1.0 and 14.7 psia. Departure diameter of more than 1,800 discrete bubbles was measured at heat fluxes up to 125,000 Btu/hr-ft^2 by a frame by frame analysis of 6,100 feet of 16 mm film taken at 3,000 and 5,000 frames per second.

The bubble diameter data were compared with analytical expressions by Owens, Ivey and Morris and Garg. An empirical expression is proposed which successfully correlates the bubble diameters in saturated nucleate pool boiling of water at all pressures. Recommendations are made to systematically investigate the effects of surface roughness and the degree of subcooling upon the bubble diameters at departure in nucleate pool boiling.

DD FORM 1 NOV 65 1473 (PAGE 1)

S/N 0101-807-6801

Unclassified

Security Classification

14 KEY WORDS	LINK A		LINK B		LINK C	
	ROLE	WT	ROLE	WT	ROLE	WT
Nucleate boiling						
Bubble diameters						
Surface roughness						
Heat transfer						

TABLE OF CONTENTS

INTRODUCTION

Boiling of a liquid on a metal surface has long been recognized as one of the best methods of obtaining very high heat transfer rates for only a few degrees temperature difference between the heating surface and the liquid. Consequently, this method of heat transfer predominates in most high power density systems. Boilers, desalination equipments, heat exchangers, boiling water nuclear reactors, and cooling of high power density electronic equipments are some of the better known applications of the boiling phenomenon. In systems like these and others, it is desirable to obtain as high a heat transfer coefficient as possible for optimum performance and for economic reasons. A limitation to the power density is, however, reached when there is a sufficient bubble density on the heating surface to cause a transition to the partial or total film boiling region.

The importance of bubble formation, growth, and departure size in determining the heat transfer characteristics of a heating surface has been discussed in detail in a recent literature survey by Garg.[1] In heat pipes employing mesh screen wicks, if the spacing between consecutive, small diameter wires was larger than the bubble diameter at departure under the heat pipe operating conditions, there is a possibility that the vapor may not be trapped in the wick thereby eliminating early dryout as a limitation of the heat pipe performance.

It was, therefore, felt that an understanding of the effect of the heating element diameter upon bubble diameter at departure over wide ranges of pressure and heat flux may add to the improved performance of heat pipes and other equipments utilizing boiling heat transfer. Consequently, an experimental investigation of saturated nucleate pool boiling was carried out to systematically determine the effects of diameter of the heating surface, pressure and heat flux upon the bubble diameters at departure. The bubble diameter data obtained during this investigation were compared with correlations found in the literature. A new empirical correlation is proposed which correlates the available bubble diameter data for water in saturated pool boiling in the discrete bubble region at all pressures.

DESCRIPTION OF THE EXPERIMENTAL APPARATUS

Test Section

Heating Element. Electrical heating was considered as the most suitable means of providing high heat fluxes on the surface of small diameter wires and tubes for this investigation. Besides the fact that there is no other practical way of heating wires of diameter as small as 0.001 inch, there are a number of advantages in using electrical heating. Among them are:

a. Heat flux is uniform.

b. High heat flux densities can be easily obtained.

c. Control and measurement of heat input rates are relatively simple and accurate.

d. The wire or tube average outer surface temperature can be easily calculated from the electrical measurements if the material of test elements has a high enough temperature coefficient of electrical resistivity.

Furthermore, spot welding a thermocouple on the outer surface of a small wire or tube to measure its temperature can cause serious distortions in the characteristics of the local surface in causing nucleate boiling and in its temperature. For these reasons, it was decided to use heating elements made of platinum. The temperature coefficient of electrical resistivity of platinum of 0.002 per degree F was considered high enough to permit accurate calculation of the outer wall temperature of the heating elements.

Seven different diameters were selected for investigating the effect of diameter of the heating surface upon the bubble diameter at departure in saturated nucleate pool boiling; viz, 0.001, 0.002, 0.005, 0.010, 0.025, 0.050, and 0.100 inch. However, the low resistances of 0.05- and 0.10- inch-diameter platinum wires requiring high input currents to obtain the heat flux levels commensurate with nucleate boiling investigations necessitated their replacement by platinum tubes of equal outer diameters.

Since the effect of surface finish upon the bubble diameter at departure was not the subject of this investigation, only smoothly drawn platinum wires and tubes were used. No effort was made to examine their surface condition. To minimize end effects due to conduction, it was decided to use approximately 6-inch heated lengths of these elements. The length to diameter ratio, therefore, varied between 60 and 6,000. To minimize the effect of disturbances caused at a location on the heating surface by bubbles departing from neighboring locations, the heating elements were mounted horizontally.

Electrical Conductors. The conductors were fabricated from 3/4-inch square section brass bars to cause negligible heat generation at the estimated maximum current of about 100 amperes, and chrome-plated to prevent contamination of water in the test tank. The heating elements were clamped to the conductors using specially designed fittings, shown in Figure 1.

Test Tank. For success in high speed photographic work, it was necessary to obtain as much transmission of light to the heating surface as possible. It was therefore decided to design a completely transparent tank. Glass and acrylic were considered. Acrylic was chosen because of the ease with which it can be machined. Based upon strength and deflection calculations, the required thickness of acrylic sheets from which the tank was fabricated was determined to be 3/4 inch.

A chrome-plated brass frame of outside dimensions 11" x 10" x 6" was fabricated by silver-brazing 1-inch-square bars at the corners and all the outside faces were machined and grooved to retain 0.125-inch-diameter rubber gaskets. To minimize leaks, machined acrylic plates were screwed to the frame to form the test tank, leak proof seals being formed by Buna-N rubber gaskets on all sides.

Penetrations for leads to measure voltage drop across the heating element, a thermocouple to measure the temperature of water in the tank, brass busbars, and connection to a manometer were provided through the top plate. A drain valve was connected to the tank through the bottom plate. Penetrations for an auxiliary heater located near the bottom of the tank to control the bulk liquid temperature were provided in the back plate. Finally, removal of vapor generated during boiling and return of the condensate were achieved through a $1\frac{1}{2}$-inch-diameter bore through the right side of the tank.

Vacuum System

The pressure range selected for this investigation was from 1.0 to 14.7 psia. The reasons for choosing this range were primarily experimental, namely,

a. Bubbles are large at low pressures. The effect of heater diameter upon the bubble diameter can be investigated with relative ease.

b. Temperatures are low which makes it possible to use acrylic for fabrication of tank, and

c. There are large changes in fluid properties over this pressure range. For instance there is a 2.4 fold change in viscosity, a 1.2 fold variation in surface tension, a 12.5 fold variation in vapor density, and 2.5 fold variation in Prandtl number.

Vacuum was created and maintained by a vacuum pump connected to the tank through the 1½-inch-diameter bore connection via a water-cooled condenser, which condensed most of the vapor generated during boiling and returned the condensate to the tank, and controlled by adjusting controlled-leak needle-valves located downstream from the condenser. A mercury manometer connected through the top plate of the tank provided accurate measurement of vacuum in the vapor space of the tank.

Power Supply

To avoid any influence of the 50 cycles per second current and voltage ripples on bubble initiation, growth or departure, it was decided to provide dc heating to the various heating elements. A Sorensen solid-state dc power supply, Model DCR20-250A, was used to provide the needed electrical power. The power unit was equipped with controls to provide continuous variation of voltage between 0 and 20 volts and that of current between 0 and 250 amperes.

A chrome-plated, inconel-sheathed, mineral-insulated resistance element of about 3 kw capacity was located at the bottom of the tank and used to raise the temperature of water in the test tank to the desired level in a short time.

Photographic Technique

Camera. A Fastex camera capable of up to 8,000 frames per second was used in this investigation with 100-foot rolls of 16 mm Eastman-4X high speed film.

Since bubble nucleation is random in both time and location on the heating surface, the choice of both the field of view and rate of boiling had to be a compromise. The field of view was largely determined by the departure size of bubbles. The bubble generation rate in the field of view had to be high enough to ensure capturing some bubbles during the short exposure time of the 100-foot rolls, and low enough to prevent gross conglomeration of bubbles and departure from nucleate boiling causing burnout of the heating element. Depending upon the pressure in the tank, an exposure speed of 3,000 or 5,000 frames per second was used.

Lighting. The lighting system consisted of two 1000-watt diffused lights located at the back of the tank and two 600-watt incandescent lights located in front of the tank. All four lights were at a 45-degree angle with the camera axis and about 10 inches away from the center of the front or back wall of the tank. On the back tankwall, in the field of view of the camera, a white ground glass was mounted to provide adequate contrast for filming. The infrared radiation from

the light sources was filtered by placing 0.5-inch-thick transparent tanks containing 5% copper sulphate solution immediately in front of the light sources. The aperture depended upon the exposure speed, the distance between camera and the heating element, and the lens used. The arrangements of lights, camera, and infrared filters in relation to the tank are shown in Figure 2. A schematic of the experimental arrangement is shown in Figure 3. Photographs of the experimental arrangement showing the various components are given in Figures 4 and 5.

METHOD OF MEASUREMENT

Heat Flux. To permit calculation of the heat flux on the outer surfaces of the various heating elements, it was necessary to accurately measure their inner and outer diameters, the heated lengths, and the voltage drop across and the current flowing through them. Details of the techniques used to measure the diameters and lengths of the various heating elements are given in Appendices A and B. Voltage drop across the heated length of each element was measured by a Leeds and Northrup, Model K-4, potentiometer through a John Fluke's Model 725A voltage divider. The voltage drop across a known resistance in series with the heating element provided the value of current flowing through it. Depending upon the current flowing through the heating element, one of the four calibrated shunt resistances was used for this measurement. The four shunts were rated at 25, 50, 100, and 300 amperes and their respective resistances were 0.002024, 0.001000, 0.00050056, and 0.00026667 ohm.

The resistivity of platinum is strongly dependent upon its purity. Therefore, it was felt necessary to carry out resistivity and temperature coefficient of resistivity measurements for each of the seven heating elements. The procedure used for these measurements and the results obtained are detailed in Appendix B.

Temperature. The temperature of water in the test tank was measured by a calibrated copper-constantan thermocouple located at the heating element level but at a distance of 1½-inch away from it in the horizontal plane. The average outer wall temperature of the heating element was determined indirectly from the voltage drop across and the current flowing through it. Allowance was made for temperature variation across the cross-section of the heating element. The procedure is described in detail in Appendix C.

Pressure. As described earlier, vacuum in the vapor space of the test tank was measured by a mercury manometer. Pressure at the heating surface was then determined from values of the barometric pressure, the height of water above the heating surface, and vacuum in the vapor space.

Bubble Diameter at Departure. Frame by frame analysis of the high speed films was carried out using a Vanguard, Model C-11D, motion picture analyser. Bubble diameters at departure from a heating surface were measured for either all bubbles appearing on a film or a limited number of bubbles considered representative of the film if there was a large number of bubbles on the film. Magnification of the actual bubble size on the projected image in the analyser was determined from fiducial marks made at a known distance apart on a stainless steel strip which was located in the field of view of the camera in the vertical plane of the heating element. For each high speed film taken, the system pressure, the heat flux on the outer surface of the heating element, the average wall to saturation temperature difference, the number of bubbles measured, and the maximum, minimum, and average departure diameters of all bubbles measured were recorded separately for each heating element.

OPERATING PROCEDURE

Assembly and Cleaning Procedure

The conductors, the platinum test element, the bulk water temperature measuring thermocouple, and leads for measuring voltage drop across the heating element were appropriately assembled and connected through the top plate of the tank. The auxiliary heater was located at the bottom of the test tank and connected to the power supply through the rear plate of the tank. All the tank faces except the front face were next screwed to the brass frame, leak proof joints being obtained by rubber gaskets on all sides and in all penetrations through the tank walls. The assembly was then thoroughly cleaned with acetone to remove traces of dirt and oil followed by several rinses with demineralized water. The front face was next screwed to the brass frame and the test tank connected to the vacuum system through the glass condenser.

The tank was filled with demineralized water to a height of about 3½ inches above the heating element, and the water heated to about 105°F using the auxiliary heater. Pressure in the tank was then reduced until the temperature of water corresponded to the saturation temperature at the pressure in the tank. Boiling was then started on the auxiliary heater and maintained for a few hours. The vapor generated during boiling was condensed in the condenser and returned to the test tank. This cleaning procedure was carried out to remove traces of dirt from the glass condenser which might enter the tank during testing. After several hours of boiling, the vacuum in the tank was broken and the water drained. The tank was next thoroughly rinsed and filled with demineralized water. This cleaning procedure was repeated several times to ensure a thoroughly clean system at the commencement of tests.

Pre-test Procedure

The test tank was filled with demineralized water to a height of about four inches above the heating element, and heated by auxiliary heater to a temperature some 4-5°F above the saturation temperature corresponding to half the test pressure. The pressure in the test tank was then reduced gradually to about half the test pressure, thereby causing bulk boiling. Water was then boiled on the heating element for about half an hour under saturated conditions to minimize the quantity of gas in the bulk liquid and that absorbed on the heating surface. Vacuum in the test tank was then broken and the water temperature raised to the saturation temperature for the test pressure by increasing the voltage drop across the auxiliary heater.

Test Procedure

Pressure in the vapor space of the test tank was reduced slowly until pressure at the heating surface corresponded to the test pressure. A small dc voltage was applied across the test element and increased slowly until boiling was observed on its surface. Power input to the element was then adjusted to obtain the desired rate of bubble formation. When steady state conditions were reached, values of current flowing through and the voltage drop across the heating element, vacuum in the vapor space above the heating element, barometric pressure, height of water above the heating surface, and bulk temperature of water were measured.

For high speed photography, the power to auxiliary heater was turned off completely just before the film run to eliminate convection currents. Lights were switched on manually just before the camera and the photographic run was carried out at the preselected speed.

DISCUSSION OF RESULTS

Observations and Comparison with Existing Correlations

Sixty-one 100-foot rolls of high speed film, taken at 3,000 and 5,000 frames per second, were analysed frame by frame using a Vanguard, Model C-11D, motion picture analyser. Bubble diameters at departure were measured at the instant of their break-off from the heating surface. These measurements were carried out for either all bubbles appearing on a film or a limited number of bubbles considered representative of the film if there was a large number of bubbles on the film. For each high speed film taken, the pressure at the heating surface (p), the heat flux on the outer surface of the heating element (q), the average outer wall to saturation temperature difference (ΔT), the number of bubbles measured, and the maximum, minimum, and arithmetic average of all bubble diameters measured are listed separately for each heating element in Tables 1 through 7. The maximum and minimum bubble departure diameter values

are included to emphasize variations caused by factors other than those considered in this investigation. Bubble diameters at departure as predicted by a number of correlations are also listed in these tables to permit comparison with the experimental data. In tabulated order, these correlations are given below. Detailed assumptions upon which derivation of these correlations are based were included earlier in a literature survey by Garg.[1]

For cylindrical heating surfaces, bubble diameters at departure in saturated pool boiling as predicted by Owens[2], Ivey and Morris[3], and Garg[4], respectively, are given by

$$D_c = \frac{d_o \rho_\ell C_\ell \Delta T}{2 \rho_v h_{fg}} \left[e^{2k\Delta T/qd_o} - 1 \right] , \qquad (1)$$

$$D_c = \frac{d_o}{2} \left[\frac{3 \rho_\ell C_\ell \Delta T}{\rho_v h_{fg}} \left\{ e^{4k\Delta T/qd_o} - 1 \right\} \right]^{\frac{1}{2}} , \qquad (2)$$

$$D_c^2 = C_c \frac{3 d_o \rho_\ell C_\ell k (\Delta T)^2}{q \rho_v h_{fg}} , \qquad (3)$$

where D_c = bubble diameter at departure from a cylindrical heating surface (ft)

d_o = outer diameter of the heating element (ft)

C_ℓ = specific heat of liquid (Btu/lb_m °F)

ρ_ℓ = density of liquid (lb_m/ft^3)

ρ_v = density of vapor (lb_m/ft^3)

h_{fg} = latent heat of evaporation (Btu/lb_m)

k = thermal conductivity of liquid (Btu/hr-ft-°F)

C_c = experimental constant for cylindrical heating surfaces which relates the thickness of the superheated layer in nucleate boiling where a bubble envelops the heating surface to its value assuming pure conduction

For cylindrical heating surfaces where the departure diameter of bubbles was less than four times the diameter of the heating surface, the departure diameter of bubbles listed in the tables is that predicted by the following equation by Garg[4] for a flat surface instead of Equation (3), as shown in Tables 6 and 7.

$$D_f = C_f \frac{3\rho_\ell C_\ell k(\Delta T)^2}{4q\rho_v h_{fg}} \quad , \tag{4}$$

where D_f = maximum bubble diameter at departure from a flat surface (ft), and C_f = experimental constant which relates the thickness of the superheated layer in nucleate boiling to its value assuming pure conduction for flat surfaces, and for cylindrical surfaces where the bubble diameter at departure is less than four times the diameter of the heating surface.

The measured average bubble diameters at departure from cylindrical heating surfaces where the bubble diameters exceeded the heating element diameter by a factor of four were converted to values which might have been obtained from flat heating surfaces under the same experimental conditions using an equation previously developed by Garg[4]:

$$D_e = \frac{C_f}{C_c} \cdot \frac{(D_c)^2_{expt}}{4d_o} \quad , \tag{5}$$

where D_e = equivalent maximum bubble diameter at departure from a flat surface (ft).

The value of C_c was determined experimentally and found to be 2.0 during experiments in saturated nucleate pool boiling at sub-atmospheric pressures from a 0.125-inch-OD tube[4]. The values of both C_c and C_f were assumed to be 2.0 for the purpose of comparisons with the predicted values. Finally, the last column in the tables lists bubble diameters at departure from flat surfaces as predicted by Patten and Garg[5], using the following equation:

$$D_f = \text{const} \left\{\frac{p_c}{p}\right\} \left[\frac{g_o\sigma}{g(\rho_\ell - \rho_v)}\right]^{\frac{1}{2}} \quad , \tag{6}$$

where p_c = critical pressure (lb_f/in^2 abs)

g_o = conversion factor (lb_m-ft/lb_f-hr^2)

σ = surface tension of liquid (lb_f/ft)

g = acceleration due to gravity (ft/hr^2).

The maximum, minimum and average values of bubble diameter at departure are plotted against the pressure at the heating surface, separately for each heating element in Figures 6 through 12 and are compared with values predicted by Equation (3). The equivalent bubble diameters at departure from a flat surface as obtained by modifying experimental data using Equation (5) are compared with the predicted values using Equation (6) in Tables 1 through 7. Before discussing the difference between the predicted and measured values, the process of bubble formation, growth and departure may be described which might help toward explaining the scatter in the data and their observed deviation from the predicted values.

a. A bubble grows by absorbing the superheat energy from the boundary layer. If after absorbing the available superheat energy a bubble has not been able to reach a large enough size to overcome the surface tension and viscous forces, it will stay attached to the heating surface and continue to grow by evaporation at the solid-liquid-vapor-interface, by conglomeration with bubbles growing in the vicinity, or both.

b. If the superheat energy in the boundary layer at bubble initiation is large enough to cause this bubble, during its growth, to exceed the size necessary to overcome the surface tension and viscous forces, the bubble may leave the heating surface even though its growth has not yet been completed.

c. The growth rate of a bubble depends upon the superheat energy available in the layer, thermodynamic and transport properties of the fluid, conglomeration with other bubbles which happen to be in the vicinity, and evaporation at the interface if the bubble has not attained a large enough size to leave the heating surface.

d. During growth, a bubble begins to move upward as soon as the buoyancy forces exceed the surface tension forces. At this time, the bubble enters into a dynamic balance with the buoyancy, viscous and surface tension forces. Before departure from the heating surface, the bubble center has to travel a sufficient distance away from the heating surface to clear the bottom of the bubble while still attached to the heating surface.

e. The total distance travelled by a bubble in a given time from its initiation will depend upon the bubble growth rate and position of the bubble on the heating surface at the time of initiation, changes in growth rate with time due to changes in the residual liquid superheat energy around the bubble, bubble activity in the vicinity and conglomeration of other bubbles into it.

f. The superheat energy in the boundary layer depends upon the waiting period and, to some extent, upon the bubble activity in its vicinity. The waiting period depends strongly upon the size and shape of surface cavities, as has been observed by a number of investigators.

Because of the many interdependent factors, especially item (f) above, it may be easily seen why bubbles vary so much in size even when externally controllable parameters like pressure, heat flux, degree of subcooling, etc., are held constant.

Observation (a) was noted with smaller diameter wires. Bubbles from certain nucleation sites were found to stay attached to the heating surface for a very long time, and continue to increase in size. For example, bubbles growing on the 0.001-inch diameter wire at atmospheric pressure were observed to stay attached to the wire for as long as 233 milliseconds. Such long attachment times were experienced by bubbles only if they did not conglomerate with other bubbles. At nucleation sites where bubbles conglomerated during their attachment to the heating surface, the attachment time was much smaller. For the larger diameter heating surfaces, the bubble diameters were much larger and the attachment time much smaller than the smaller diameter heating surfaces. For the largest diameter heating surface, it appeared that observation (b) may well apply.

The somewhat large deviation of bubble diameters from values predicted by Equation (3) shown in Figures 6 and 7 may be explained by the fact that during derivation of the equation, it was assumed in the interest of simplicity that the thickness of the superheated boundary layer in boiling is small compared to the diameter of the heating surface. This assumption becomes less valid as the lowest diameter of the heating surface of 0.001 inch is approached. Furthermore, it may be noted that this equation was obtained from a simple energy balance and as such does not consider factors to satisfy bubble departure requirements. Therefore, for small diameter wires at higher pressures, the superheat energy in the boundary layer may not be enough to produce large enough bubbles, resulting in their staying attached to the heating surface until they can grow to a sufficient size prior to departure, as described in observation (a). For tubes of 0.0506 and 0.100-inch OD, the exact opposite may well have begun to hold true, as described in observation (b), as the lowest pressure is approached. This observation may offer an explanation for measured bubble diameters in some cases to be somewhat smaller than the values predicted by Equations (3) and (4).

As the system pressure is increased above the atmospheric pressure, it is easy to envision that bubble growth rates will be reduced significantly because of two factors; lower wall-to-saturation temperature drops in boiling which will limit the superheat energy in the boundary layer, and higher vapor densities causing a smaller final size for the same superheat energy. Under such conditions, it is highly probable that the growth due to energy in the boundary layer plays a progressively lesser part in determining the final size at departure. The well known Fritz[6] equation may well begin to become important in determining bubble sizes at departure at the higher pressures. However, since the Fritz correlation does not make allowance for either the heat transfer which causes bubbles to grow large at the low pressures or the dynamic nature of the boiling process which might cause bubbles to depart before the available superheat energy in the boundary layer has been completely absorbed by the bubble, it is anticipated that bubble diameters at departure may well be above or below the values predicted by the Fritz correlation. A combination of the Fritz correlation with consideration of the superheat energy in the boundary layer may well offer a better correlation.

Equations (1) to (5) are based only upon an energy balance between the superheated liquid layer and the bubble, and they do not include the requirement that a bubble has to continue to grow to a large enough size to be able to overcome the surface tension and viscous forces prior to its departure from the heating surface. An examination of Figures 6 to 12 and Tables 1 to 7 shows that, despite this limitation and the unavoidable scatter of data, these equations are much more successful in predicting bubble diameters than the Fritz correlation. This suggests that the superheat energy in the boundary layer in these experiments must have been a much more significant factor in determining bubble diameters at departure compared to the effects of buoyancy and surface tension forces, at least at the lower pressures. Some adjustment in these equations to include the presence and the requirement of a sufficient buoyancy force is needed for predictions at the higher pressures.

The two factors discussed above viz, (1) the assumption of thickness of the boundary layer being small compared to the diameter of the heating surface and, (2) the bubble departure requirements, may explain the observed increase in deviation between the predicted and the measured bubble diameters as the heating element diameter decreases. This was especially true at the higher pressures where bubbles stayed attached to the heating surface and kept growing until they reached a large enough size to permit departure from the heating surface.

The systematic effects of system parameters considered as variables in this experimental investigation will now be discussed.

Effect of Diameter of the Heating Surface

Bubble diameters at departure from a heating surface at a particular pressure were averaged for all heat fluxes and plotted against diameter of the heating element, separately for each pressure in Figure 13. This was done because, as will be shown later, the effect of heat flux upon bubble diameter was undetectably small compared to variations caused by factors other than those considered in this investigation. Also shown in the figure for comparison is the dependence of bubble diameter upon heating element diameter as predicted by Equation (3), viz.,

$$D_c \propto d_o^{\frac{1}{2}} \quad .$$

If allowance is made for the observation discussed earlier that bubbles from smaller diameter wires were much larger because of the departure requirements, the data approximately support the dependence predicted by Equation (3).

Effect of Pressure

Average bubble diameters at departure are plotted against pressure separately for each heating element in Figure 14. As may be seen, the bubble diameter decreases with an increase in the system pressure. Although there is no pressure term in Equation (3), its presence is well accounted for through its effect upon the properties of liquid and vapor. A more direct inclusion of the pressure term in a correlation was carried out in Equation (6).

As shown later, a correlation of all data was carried out by combining Equation (3) with the Fritz correlation to include the effect of buoyancy and surface tension forces.

Effect of Heat Flux

To determine the systematic effect of heat flux upon the bubble diameter at departure, the ratio of average bubble diameters at departure for the highest and lowest heat flux values was compared with the ratio of the highest and the lowest heat fluxes. These ratios are tabulated for all wires and tubes at all system pressures in Table 8. Also given in this table for comparison is the highest value of the ratio of maximum and minimum bubble diameters at a given heat flux. In Table 8, therefore

$$B_1 = \frac{\text{Average } (D_c)_{expt} \text{ for the highest q}}{\text{Average } (D_c)_{expt} \text{ for the lowest q}} \quad , \qquad (7)$$

$$B_2 = \frac{\text{Highest value of q}}{\text{Lowest value of q}} \quad , \tag{8}$$

$$B_3 = \frac{\text{Maximum } (D_c)_{expt}}{\text{Minimum } (D_c)_{expt}} \quad , \text{ at a given q.} \tag{9}$$

It may be seen from the values of ratio B_3 in Table 8 that, for a given set of experimental conditions (pressure at the heating surface, diameter of the heating element, surface orientation, average heat flux, height of water above the heating surface, and the degree of subcooling which was zero in the work reported here), the variation in bubble diameter at departure was as high as X4.10 for the 0.100-inch-OD tube at 3.0 psia. It may also be noted that with this one exception in the value of ratio B_3 of 4.10 for the 0.100-inch-OD tube at 3.0 psia, the ratio B_3 decreases as the system pressure is increased. This anomaly was apparently caused by large waiting periods on the entire tube surface followed by explosive growth of large bubbles at a specific location on the heating surface. At departure, these large bubbles left vapor tails on the tube surface which grew into trails of smaller bubbles from these locations. The former, parent bubbles were perhaps the result of nucleation of a surface cavity which required a higher wall superheat, thereby a larger superheat energy at bubble initiation, whereas the streams of bubbles following these large bubbles were probably caused by evaporation at the boundary of the pre-existing gaseous phase. These latter bubbles had very little waiting period and smaller attachment time to the heating surface compared to the parent bubbles. It was perhaps this difference in nucleation of a surface cavity in one case and evaporation into the pre-existing gaseous phase in the other which caused such large differences in their departure sizes.

Variations in bubble size at departure could be caused by a combination of several factors. Besides the waiting period and the attachment time of the bubble to the heating surface discussed above, other important parameters which may affect maximum bubble size are: variations in the size, shape and density of cavities in the heating surface, the bubble growth rate and the dynamics of bubbles growing in the vicinity.

In order to evaluate the effect of heat flux upon bubble diameter at departure, two factors will now be examined. First, the ratio B_1 which was found to be below 1.00 for 11 of the 23 test conditions indicating that an increase in heat flux reduces the bubble diameter at departure, and above 1.00 for the other 12 test conditions indicating exactly the opposite. Second, with one exception the variation of

ratio B_1 above and below 1.00 was found to be much smaller than variation in bubble diameter at departure indicated by the ratio B_3. An examination of these two factors indicates little if any effect of heat flux upon the maximum bubble diameter at departure. It may well be that the heat flux does have some systematic effect upon the bubble diameter; however, in view of the large values of ratio B_3, its determination will have to wait until the effects of parameters other than those considered in this work upon the bubble diameter at departure are systematically determined. For this analysis, therefore, the effect of heat flux will be considered to be negligible. This observation is in agreement with the work of Gaertner and Westwater[7] and Hatton and Hall.[8]

Correlation of Experimental Data

If the above observation of negligible effect of heat flux on bubble diameter at departure is assumed to be reasonably accurate over the entire discrete bubble region at a given pressure, and since only one of heat flux or wall to bulk temperature difference is independently variable at a constant pressure, the heat flux may be assumed to be proportional to the square of the wall to bulk temperature difference, or

$$q = C_1 (\Delta T)^2 \quad . \tag{10}$$

If Equation (10) can be combined with Equations (3) and (4), the need for experimental measurements in predicting bubble diameters at departure may be eliminated. However, some allowance has to be made for this constant of proportionality which, although assumed a constant over the entire discrete bubble region at a given pressure, is not a constant for all pressures This adjustment may be carried out as follows. Since all the liquid and vapor properties used in Equations (3) and (4) vary with pressure, the variation in the value of C_1 may be accounted for by changing the index of all the properties combined. Therefore, Equations (3) and (4) modified by Equation (10) may be written as

$$D_c^2 = 3 d_o C_c \left[\frac{\rho_\ell C_\ell k}{C_1 \rho_v h_{fg}} \right]^{C_2} \quad , \tag{11}$$

and

$$D_f = \frac{3}{4} C_f \left[\frac{\rho_\ell C_\ell k}{C_1 \rho_v h_{fg}} \right]^{C_2} , \qquad (12)$$

where C_1 and C_2 are experimental constants. Combining Equations (11) and (12) leads to

$$D_f = \frac{C_f}{C_c} \cdot \frac{D_c^2}{4d_o} , \qquad (13)$$

which is of the same form as Equation (5) and may be used to convert bubble diameters at departure from cylindrical surfaces into equivalent bubble diameters at departure from flat surfaces.

To include the effects of buoyancy and surface tension forces which determine the bubble departure requirements, and assuming the contact angle to be constant at all pressures[9], Equation (12) may be modified by the Fritz expression to give

$$D_f = \frac{3}{4} C_3 C_f \left[\frac{\rho_\ell C_\ell k}{C_1 \rho_v h_{fg}} \right]^{C_2} \left[\frac{g_o \sigma}{g(\rho_\ell - \rho_v)} \right]^{\frac{1}{2}} , \qquad (14)$$

where C_3 is a constant. Equation (14) may be simplied to

$$D_f = C_4 \left[\frac{\rho_\ell C_\ell k}{\rho_v h_{fg}} \right]^{C_2} \left[\frac{g_o \sigma}{g(\rho_\ell - \rho_v)} \right]^{\frac{1}{2}} , \qquad (15)$$

where C_4 is a dimensional constant.

All experimentally obtained bubble diameters at departure for water from cylindrical wires and tubes where the bubble diameter exceeded the diameter of the heating surface by a factor of four were

modified using Equation (5) and compared with Equation (15) in Figure 15. Experimental data from other authors[4,8-15] for water taken in the discrete bubble region were also inserted in the figure, and a suitable value for C_2 was found to be 1.05. The value of constant C_4 will depend upon the units used in Equation (15). The large spread of data in Figure 15 is not unexpected because,

a. the heat flux is not always proportional to the square of wall superheat,

b. the size, shape and distribution of cavities on the heating surface have a large effect upon the superheat energy in the boundary layer at the time of bubble initiation through their effects upon the waiting period,

c. the thickness of the boundary layer and the temperature gradient in it in boiling cannot be accurately predicted by the use of a simple conduction equation,

d. heat flux and wall to saturation temperature difference in boiling are not static quantities, and they vary greatly in time and location on the heating surface, and

e. bubble activity in the vicinity of a nucleation site has a significant effect upon its nucleation characteristics and upon bubble growth and departure characteristics.

Since not one of the above five can be quantified in a meaningful manner, accurate prediction of bubble diameter is extremely difficult. Nevertheless, attempts to at least determine the gross effects of the thermodynamic and transport properties of the liquid and vapor have to be made. Hopefully, Equation (15) is a step in the right direction.

The next step is to experimentally investigate the gross effects of roughness of the heating surface and small variations in bulk temperatures from the saturation temperature upon the bubble diameters at departure.

CONCLUSIONS

A high speed photographic study of saturated nucleate pool boiling of water was carried out from horizontally mounted wires and tubes of diameter between 0.001 and 0.100 inch at subatmospheric pressures. Based upon the frame by frame analysis of films, the following conclusions were reached.

a. The bubble diameter at departure may be determined from an energy balance in the superheated boundary layer, with some consideration for the buoyancy and surface tension forces which control bubble departure.

b. The diameter of a bubble at departure is approximately proportional to the square root of the heating surface diameter for tests where the bubble diameter at departure exceeds the heating surface diameter by a factor of four.

c. An increase in the system pressure decreases the diameter of the bubble at departure.

d. There is no systematic effect of heat flux upon the diameter of bubbles at departure in the discrete bubble region.

e. An empirical equation is proposed which successfully correlates all the available data on bubble diameters at departure in saturated nucleate pool boiling of water at all pressures.

RECOMMENDATIONS

A systematic experimental investigation should be carried out to determine the effects of surface roughness and small variations in bulk temperature from the saturation temperature upon the bubble diameters at departure in pool boiling.

Table 1. Data for Saturated Pool Boiling of Water for a Wire of Diameter 0.001 Inch

p psia	q 10^4 Btu/hr-ft^2	ΔT ^oF	No. of bubbles measured	$(D_c)_{expt}$ Max. 10^{-3}ft	$(D_c)_{expt}$ Min. 10^{-3}ft	$(D_c)_{expt}$ Aver. 10^{-3}ft	$(D_c)_{pred}$ Eqn. (1) 10^{-3}ft	$(D_c)_{pred}$ Eqn. (2) 10^{-3}ft	$(D_c)_{pred}$ Eqn. (3) 10^{-3}ft	D_e Eqn. (5) 10^{-3}ft	D_f Eqn. (6) 10^{-3}ft
3.0	12.5	72.8	36	7.30	4.43	5.68	3393	258.6	7.90	90.5	81
7.0	5.65	22.6	9	5.96	5.34	5.58	106.8	22.1	2.97	87.1	34.5
7.0	7.72	25.2	27	6.50	4.16	5.65	60.8	12.3	2.38	89.5	34.5
14.7	6.71	22.3	20	6.61	4.44	5.17	29.4	8.88	1.61	74.9	15.6
14.7	8.01	23.6	34	6.10	4.32	5.22	21.9	6.53	1.78	76.4	15.6

Table 2. Data for Saturated Pool Boiling of Water for a Wire of Diameter 0.002 Inch

p psia	q 10^4 Btu/hr-ft^2	ΔT ^oF	No. of bubbles measured	$(D_c)_{expt}$ Max. 10^{-3}ft	$(D_c)_{expt}$ Min. 10^{-3}ft	$(D_c)_{expt}$ Aver. 10^{-3}ft	$(D_c)_{pred}$ Eqn. (1) 10^{-3}ft	$(D_c)_{pred}$ Eqn. (2) 10^{-3}ft	$(D_c)_{pred}$ Eqn. (3) 10^{-3}ft	D_e Eqn. (5) 10^{-3}ft	D_f Eqn. (6) 10^{-3}ft
7.0	6.14	23.3	36	7.86	5.50	6.46	31.2	6.0	3.38	62.6	34.5
7.0	9.16	26.5	36	7.31	4.85	6.17	20.8	5.04	3.14	57.1	34.5
14.7	3.35	16.0	17	6.46	5.00	5.90	18.8	7.06	2.24	52.2	15.6
14.7	5.08	26.4	36	6.88	4.83	5.64	38.7	11.1	3.00	47.7	15.6

Table 3. Data for Saturated Pool Boiling of Water for a Wire of Diameter 0.005 Inch

p psia	q 10^4 Btu/ hr-ft^2	ΔT ^oF	No. of bubbles measured	$(D_c)_{expt}$ Max. 10^{-3}ft	$(D_c)_{expt}$ Min. 10^{-3}ft	$(D_c)_{expt}$ Aver. 10^{-3}ft	$(D_c)_{pred}$ Eqn. (1) 10^{-3}ft	$(D_c)_{pred}$ Eqn. (2) 10^{-3}ft	$(D_c)_{pred}$ Eqn. (3) 10^{-3}ft	D_e Eqn. (5) 10^{-3}ft	D_f Eqn. (6) 10^{-3}ft
1.0	6.63	41.2	22	19.2	8.3	15.3	337	28.9	21.6	138.6	247
1.0	7.65	38.3	41	16.9	8.2	11.9	224	21.8	18.7	86.4	247
3.0	7.24	35.9	57	14.0	6.92	10.1	79.7	13.2	11.1	61.2	81
3.0	9.06	35.2	30	12.0	6.60	8.80	54.8	10.2	9.69	46.5	81
7.0	2.43	19.5	9	10.3	6.84	8.81	46.7	12.7	7.15	46.5	34.5
7.0	5.02	24.8	36	9.50	6.81	7.94	25.9	7.6	6.27	37.8	34.5
14.7	2.75	16.8	22	9.10	7.10	7.75	12.6	3.3	4.09	36.0	15.6
14.7	5.19	40.0	36	8.43	5.63	7.18	45.6	12.3	7.09	31.2	15.6

Table 4. Data for Saturated Pool Boiling of Water for a Wire of Diameter 0.010 Inch

p psia	q 10^4 Btu/hr-ft^2	ΔT ^oF	No. of bubbles measured	$(D_c)_{expt}$ Max. 10^{-3}ft	$(D_c)_{expt}$ Min. 10^{-3}ft	$(D_c)_{expt}$ Aver. 10^{-3}ft	$(D_c)_{pred}$ Eqn. (1) 10^{-3}ft	$(D_c)_{pred}$ Eqn. (2) 10^{-3}ft	$(D_c)_{pred}$ Eqn. (3) 10^{-3}ft	D_e Eqn. (5) 10^{-3}ft	D_f Eqn. (6) 10^{-3}ft
1.0	7.66	52.1	13	49.6	22.0	36.9	352	35.2	36.0	387	247
3.0	4.09	33.5	48	20.0	9.5	11.8	112	20.9	19.5	41.6	81
3.0	4.70	32.0	40	19.2	9.4	13.3	82.9	17.3	17.3	52.8	81
7.0	2.63	12.7	48	10.3	6.76	8.11	9.94	5.66	6.29	19.6	34.5
7.0	5.65	19.6	36	9.0	5.73	6.83	10.3	5.55	6.62	13.8	34.5
14.7	2.72	17.2	35	8.75	6.38	7.41	9.71	5.86	5.97	16.3	15.6
14.7	5.16	16.3	36	9.46	6.25	8.27	3.91	3.40	4.11	20.4	15.6

Table 5. Data for Saturated Pool Boiling of Water for a Wire of Diameter 0.026 Inch

p psia	q 10^4 Btu/hr-ft^2	ΔT ^oF	No. of bubbles measured	$(D_c)_{expt}$ Max. 10^{-3}ft	$(D_c)_{expt}$ Min. 10^{-3}ft	$(D_c)_{expt}$ Aver. 10^{-3}ft	$(D_c)_{pred}$ Eqn. (1) 10^{-3}ft	$(D_c)_{pred}$ Eqn. (2) 10^{-3}ft	$(D_c)_{pred}$ Eqn. (3) 10^{-3}ft	D_e Eqn. (5) 10^{-3}ft	D_f Eqn. (6) 10^{-3}ft
1.0	2.33	47.4	6	63.7	33.7	47.0	1011	98.9	95.4	255	247
1.0	3.74	39.5	37	57.1	21.3	34.6	365	53.6	62.8	138	247
1.0	5.09	44.9	52	45.3	20.5	29.8	336	50.6	61.2	103	247
3.0	2.68	39.0	25	33.0	22.8	28.4	204	42.0	45.0	93	81
3.0	4.16	41.4	58	35.0	16.7	26.0	135	32.6	38.3	78.2	81
3.0	5.46	36.9	47	31.1	13.9	21.3	77.4	23.9	29.8	52.5	81
7.0	1.24	19.5	24	15.9	10.3	12.1	52.9	21.8	22.6	17.0	34.5
7.0	2.74	24.5	34	17.5	12.3	14.8	33.2	16.0	19.1	25.2	34.5
14.7	1.38	19.6	36	14.6	10.1	11.8	24.8	14.7	15.7	16.0	15.6
14.7	2.96	26.6	35	16.0	12.1	14.0	18.5	12.0	14.2	22.7	15.6

Table 6. Data for Saturated Pool Boiling of Water for a Tube of Diameter 0.0506 Inch

p psia	q 10^4 Btu/hr-ft^2	ΔT ^oF	No. of bubbles measured	$(D_c)_{expt}$ Max. 10^{-3}ft	$(D_c)_{expt}$ Min. 10^{-3}ft	$(D_c)_{expt}$ Aver. 10^{-3}ft	$(D_c)_{pred}$ Eqn. (1) 10^{-3}ft	$(D_c)_{pred}$ Eqn. (2) 10^{-3}ft	$(D_c)_{pred}$ Eqn. (3) 10^{-3}ft	D_e Eqn. (5) 10^{-3}ft	D_f Eqn. (6) 10^{-3}ft
1.0	2.62	31.3	1	*	*	92.3	303	65.3	83.0	502	247
1.0	3.42	28.2	32	76.3	29.3	48.2	181	49.8	65.5	138	247
1.0	4.49	24.7	32	68.5	21.5	45.7	104	37.2	50.0	124	247
3.0	1.54	13.9	36	34.1	12.7	17.8	37.5	22.7	29.6	18.8	81
3.0	2.17	17.4	36	26.2	12.7	19.0	41.2	23.7	31.1	21.4	81
3.0	3.47	18.5	36	38.3	16.7	24.0	28.3	19.4	26.2	34.0	81
7.0	1.22	16.5	36	15.4	9.83	12.6	32.5	21.7	43.0+	12.6*	34.5
7.0	2.26	22.9	36	18.8	11.9	14.8	32.7	21.4	44.5+	14.8*	34.5
7.0	4.04	26.8	36	24.7	17.3	21.0	24.3	18.1	24.0	26.0	34.5
14.7	1.63	14.7	36	16.4	12.2	13.8	9.42	11.4	13.0+	13.8*	15.6
14.7	2.48	17.8	24	17.0	12.4	15.7	8.93	11.0	12.5+	15.7*	15.6

+ Obtained from Equation (4) because the bubble diameter was less than 4 times the diameter of the heating surface.

* Same as experimentally measured diameter since it was less than 4 times the diameter of the heating surface.

Table 7. Data for Saturated Pool Boiling of Water for a Tube of Diameter 0.100 Inch

p psia	q 10^4 Btu/hr-ft^2	ΔT ^oF	No. of bubbles measured	$(D_c)_{expt}$ Max. 10^{-3}ft	$(D_c)_{expt}$ Min. 10^{-3}ft	$(D_c)_{expt}$ Aver. 10^{-3}ft	$(D_c)_{pred}$ Eqn. (1) 10^{-3}ft	$(D_c)_{pred}$ Eqn. (2) 10^{-3}ft	$(D_c)_{pred}$ Eqn. (3) 10^{-3}ft	D_e Eqn. (5) 10^{-3}ft	D_f Eqn. (6) 10^{-3}ft
1.0	2.42	37.8	8	130	51.7	108	461	111	146.5	350	247
1.0	4.03	33.0	22	118	60.5	79.7	204	72.7	99.3	191	247
1.0	5.53	32.1	34	85.0	45.8	61.3	139	59.8	82.5	113	247
3.0	1.30	20.6	17	59.0	14.4	26.4	96.4	51.0	133+	26.4*	81
3.0	2.35	21.5	53	49.8	14.8	24.0	56.4	38.4	81+	24.0*	81
3.0	3.56	24.8	31	51.7	28.3	40.8	49.0	35.5	48.6	50.0	81
7.0	0.71	13.9	36	18.2	13.2	16.0	38.4	32.5	52.5+	16.0*	34.5
7.0	1.19	14.8	36	23.8	15.9	19.0	25.1	25.8	35.4+	19.0*	34.5
7.0	1.80	18.1	24	25.3	19.1	22.2	24.5	25.3	35.2+	22.2*	34.5
14.7	0.83	9.5	36	18.4	14.8	16.3	7.5	14.1	10.6+	16.3*	15.6
14.7	1.33	12.0	36	20.0	15.9	18.0	7.35	13.9	10.6+	18.0*	15.6
14.7	1.87	13.4	36	23.9	17.8	22.0	6.48	13.0	9.4+	22.0*	15.6

+ Obtained from Equation (4) because the bubble diameter was less than 4 times the diameter of the heating surface.

* Same as experimentally measured diameter since it was less than 4 times the diameter of the heating surface.

Table 8. Data for the Determination of the Effect of Heat Flux Upon Bubble Diameter at Departure

Heater dia. (in.)	Ratio	Pressure, psia			
		1.0	3.0	7.0	14.7
0.001	B_1	*	*	1.01	1.01
	B_2	*	*	1.37	1.20
	B_3	*	1.65	1.56	1.49
0.002	B_1	*	*	0.95	0.96
	B_2	*	*	1.49	1.52
	B_3	*	*	1.51	1.42
0.005	B_1	0.71	0.87	0.90	0.93
	B_2	1.15	1.25	2.06	1.88
	B_3	2.31	2.02	1.51	1.50
0.010	B_1	*	1.13	0.84	1.12
	B_2	*	1.15	2.14	1.90
	B_3	2.26	2.10	1.57	1.51
0.026	B_1	0.63	0.75	1.22	1.19
	B_2	2.18	2.04	2.21	2.14
	B_3	2.68	2.24	1.54	1 45
0.0506	B_1	0.95	1.35	1.67	1.14
	B_2	1.31	2.26	3.31	1.52
	B_3	3.19	2.68	1.58	1.37
0.100	B_1	0.57	1.55	1.39	1.20
	B_2	2.28	2.74	2.54	2.25
	B_3	2.51	4.10	1.50	1.34

* Data not available.

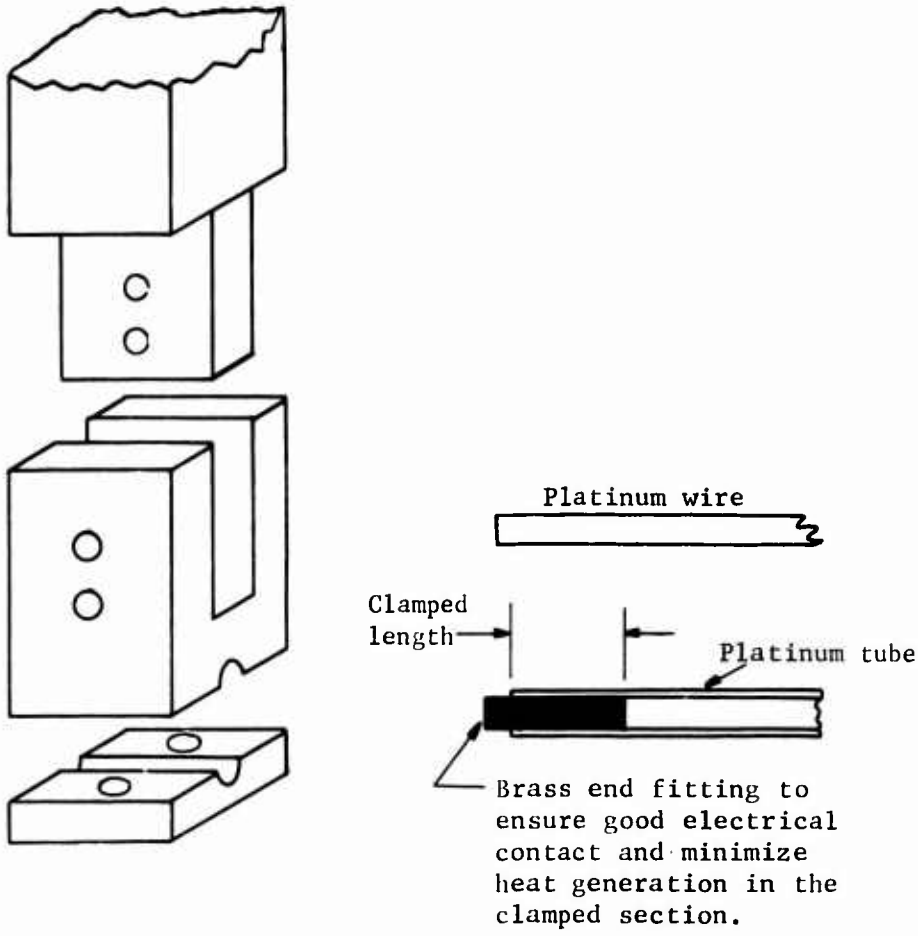

Fig. 1. Clamp connection between the heated element and brass busbars.

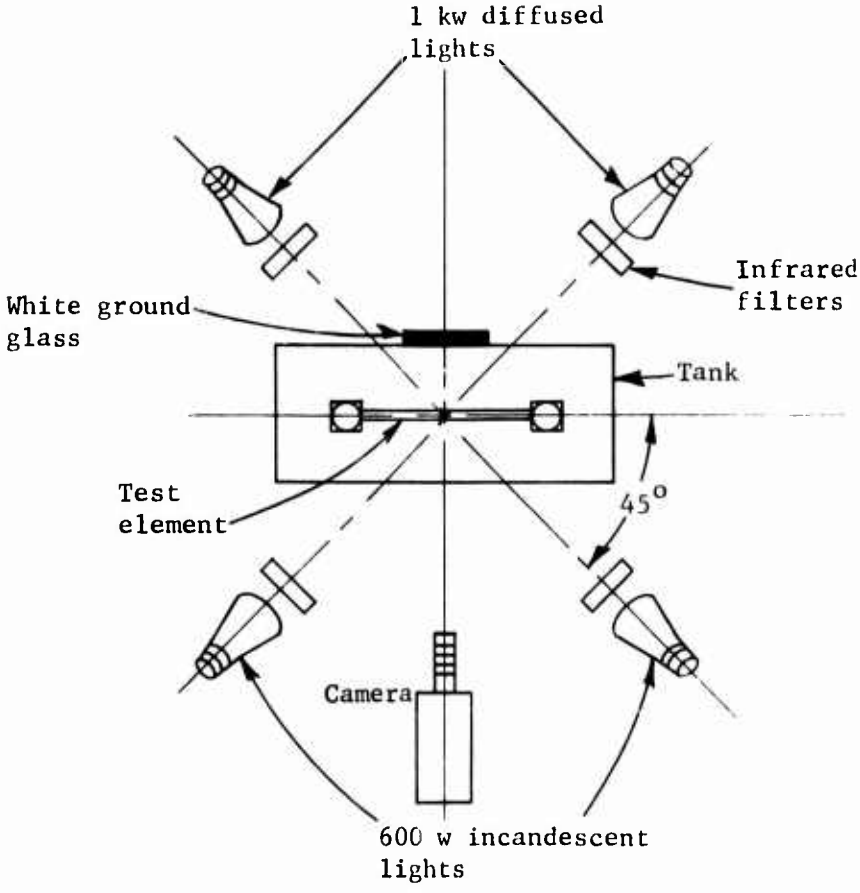

Fig. 2. Arrangement of lights and camera for high speed photography.

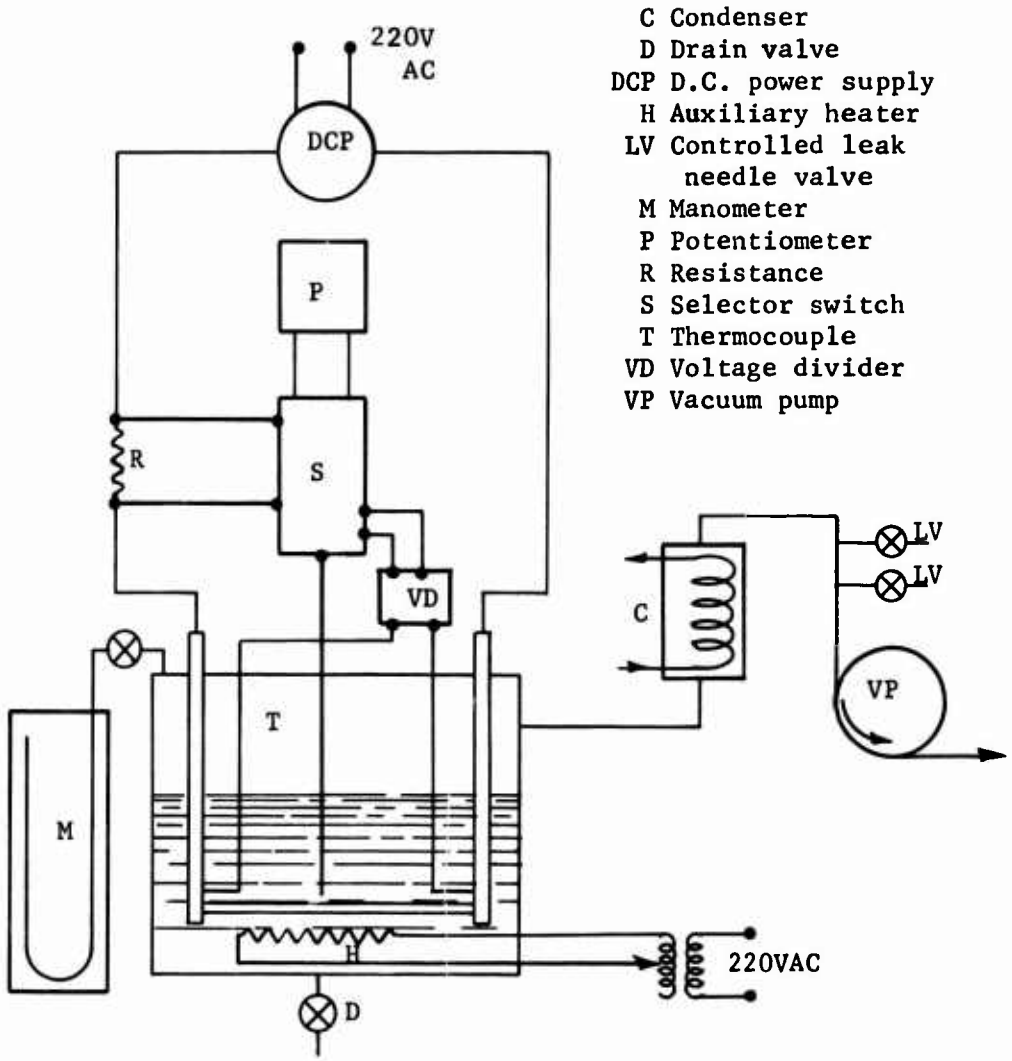

Fig. 3. Schematic of the experimental arrangement.

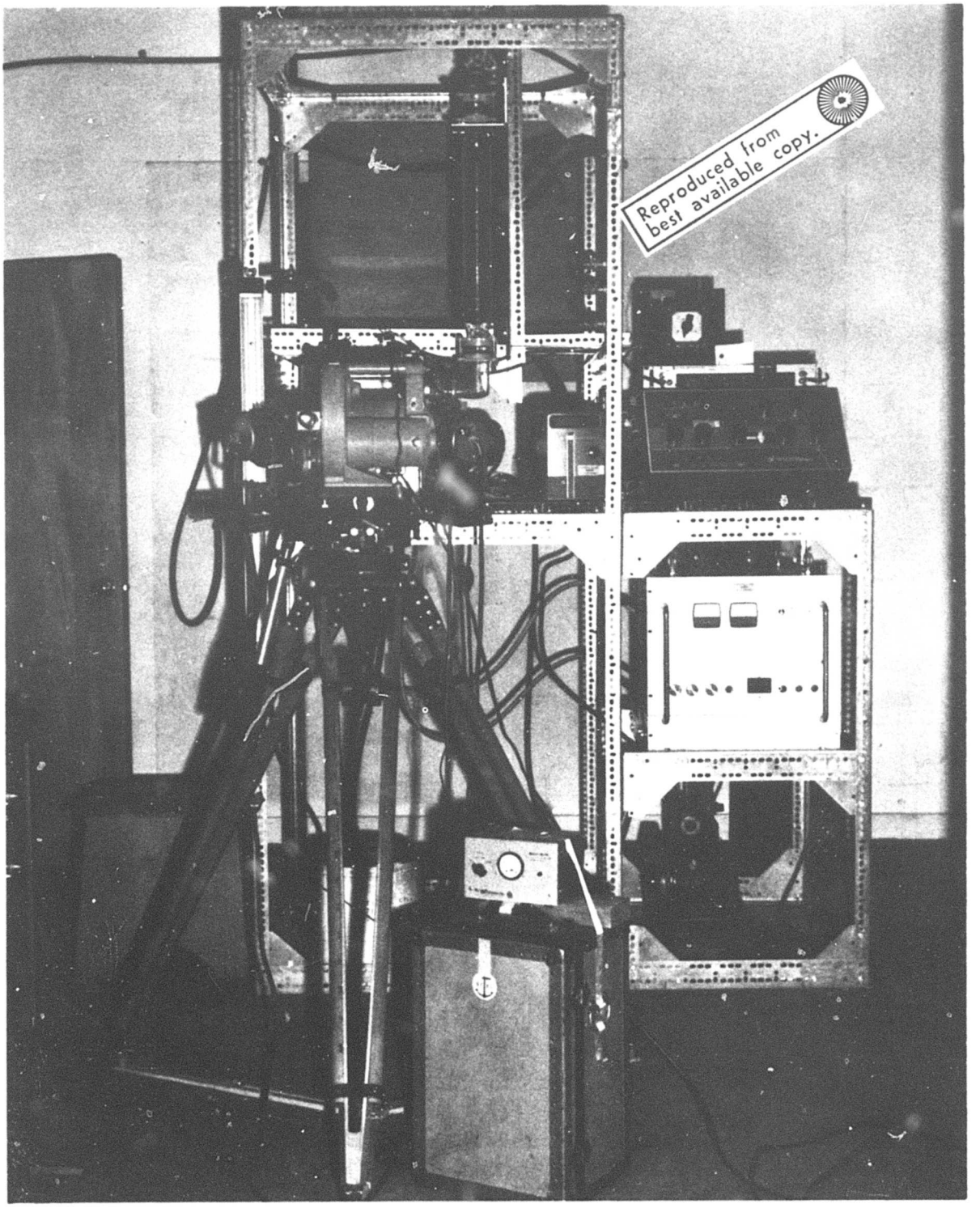

Fig. 4. Photograph of the experimental arrangement.

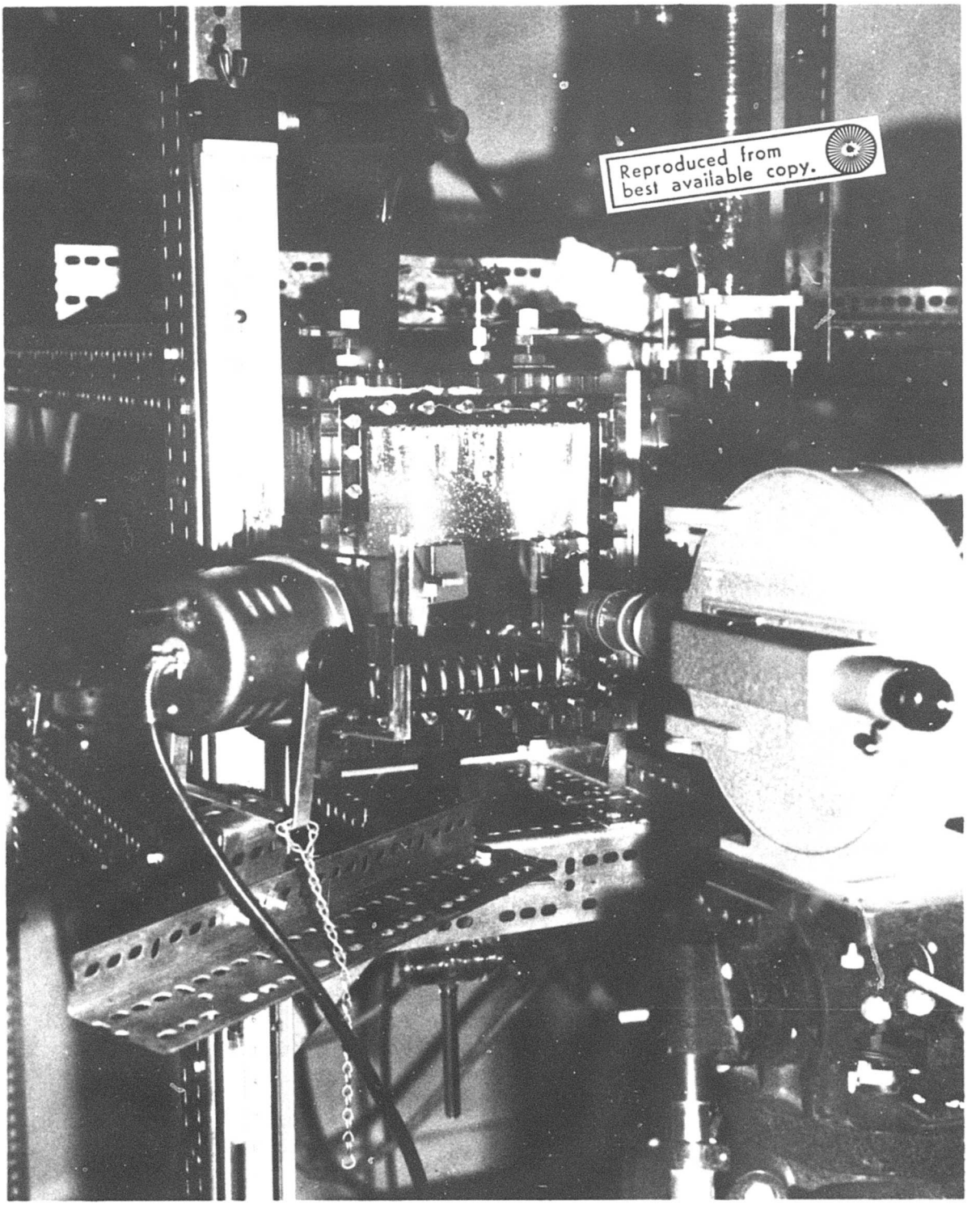

Fig. 5. Photograph of the experimental arrangement.

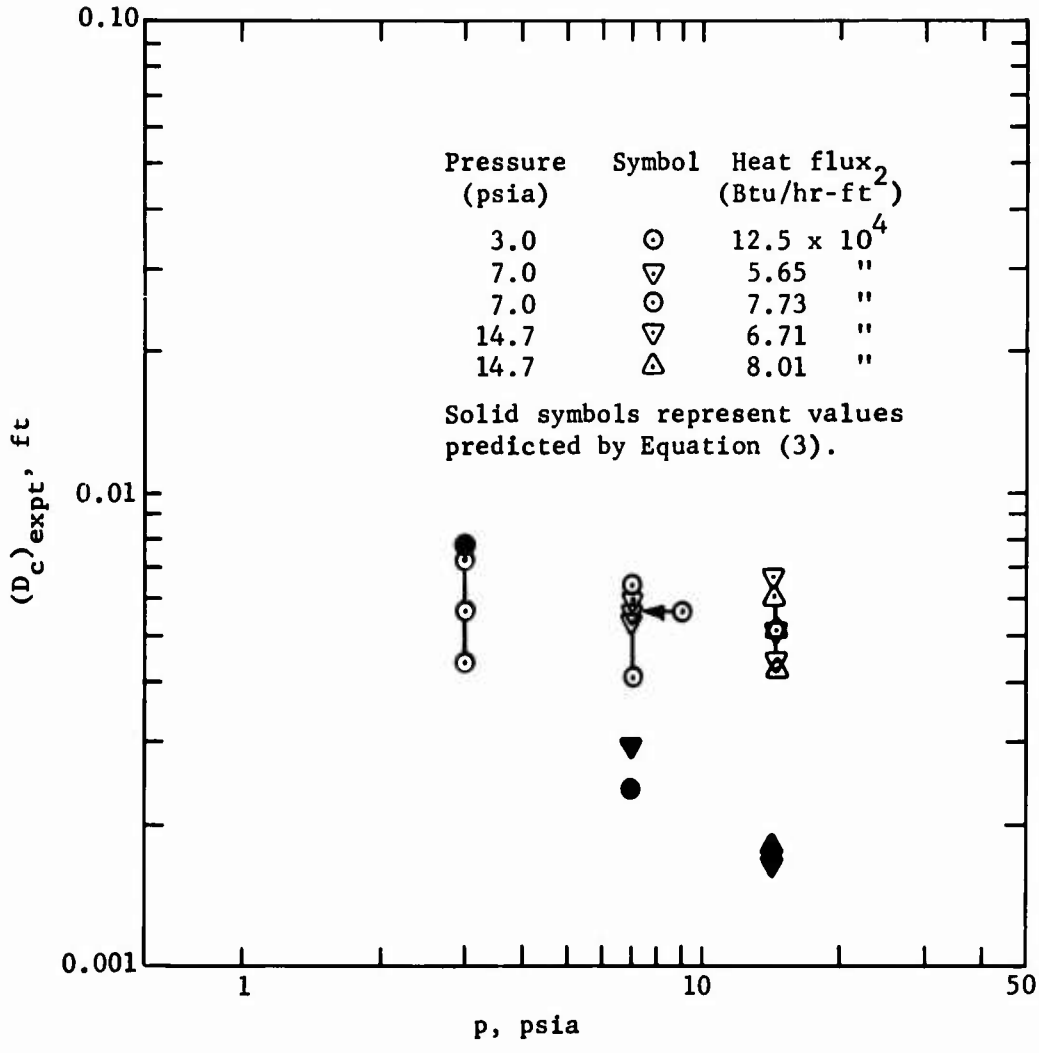

Fig. 6. Maximum, minimum and average values of bubble diameters at departure from 0.001-inch-diameter wire at various pressures and heat fluxes.

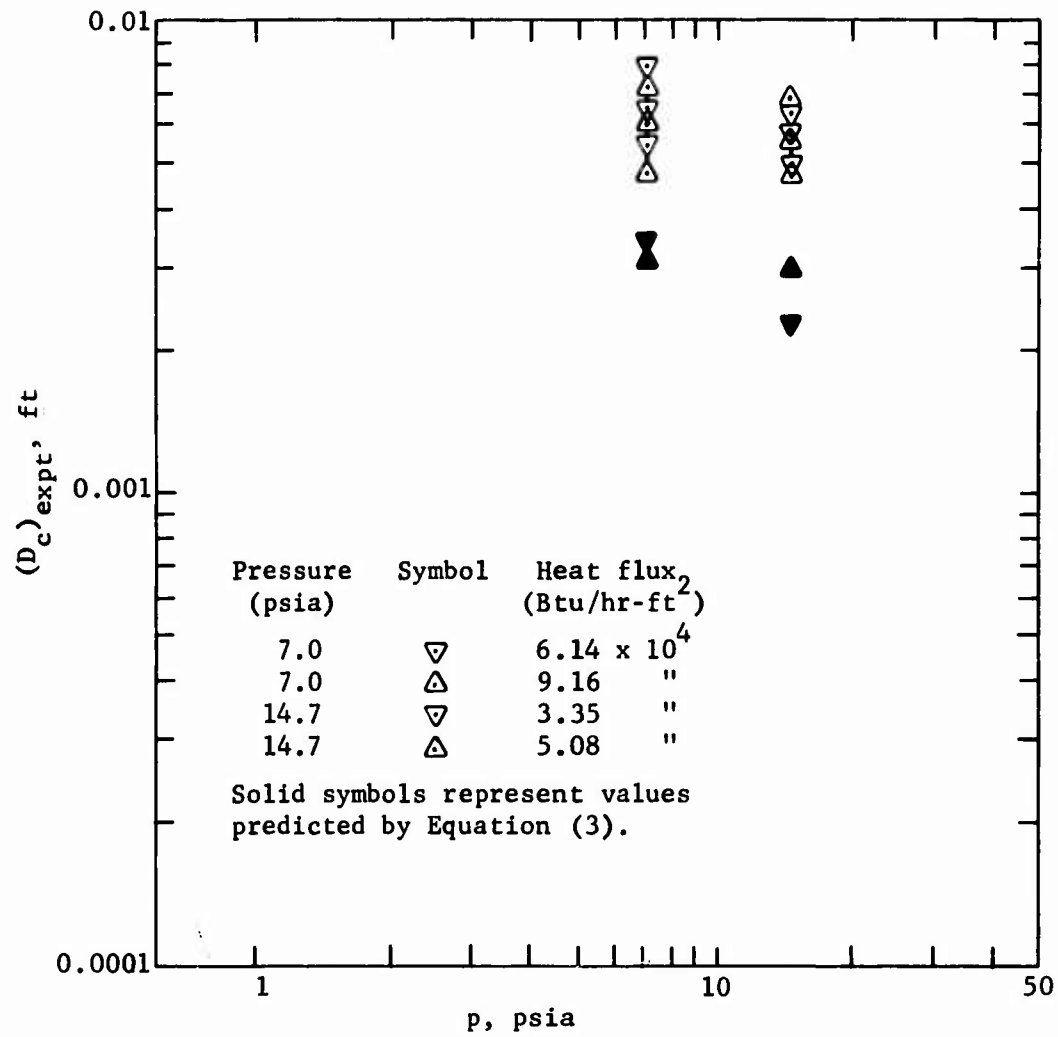

Fig. 7. Maximum, minimum and average values of bubble diameters at departure from 0.002-inch-diameter wire at various pressures and heat fluxes.

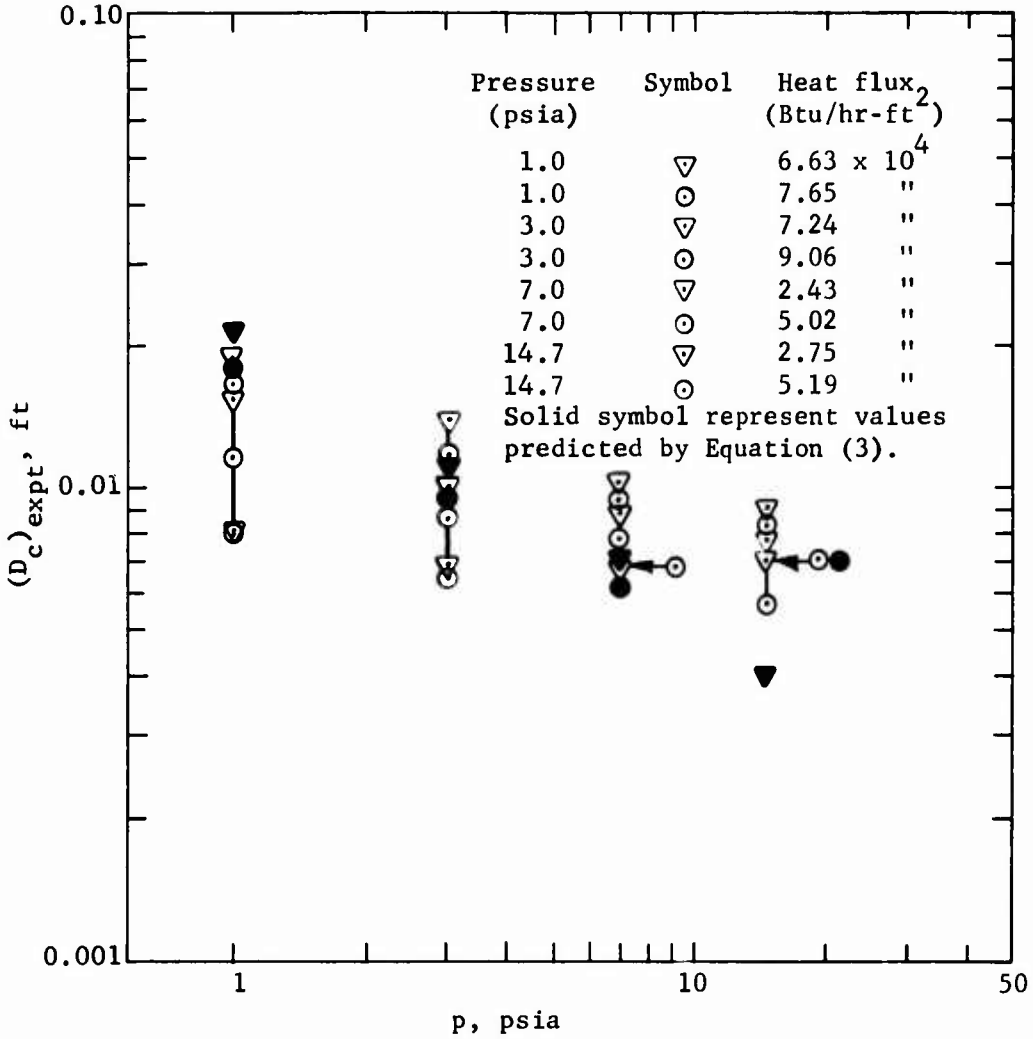

Fig. 8. Maximum, minimum and average values of bubble diameters at departure from 0.005-inch-diameter wire at various pressures and heat fluxes.

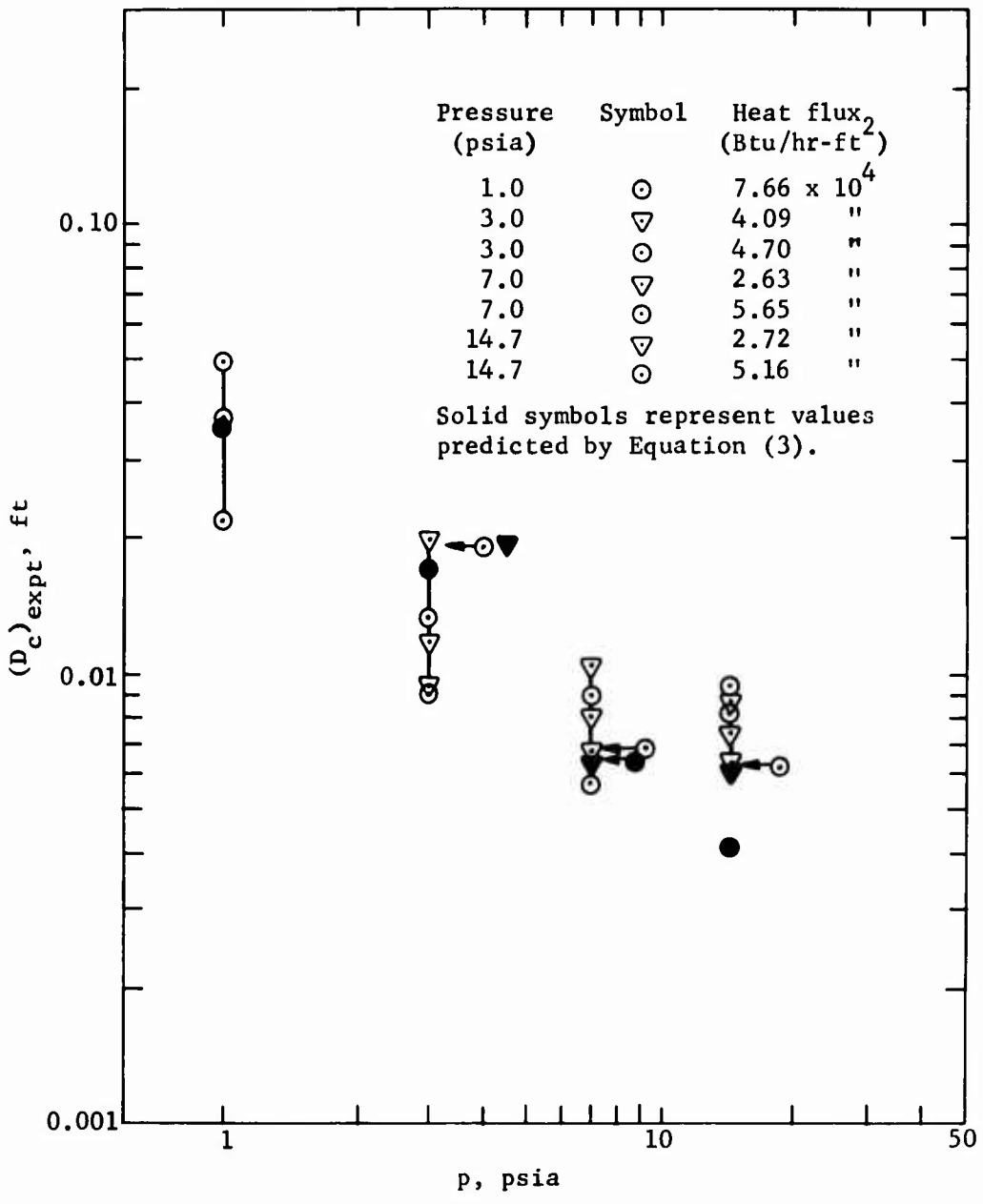

Fig. 9. Maximum, minimum and average values of bubble diameters at departure from 0.01-inch-diameter wire at various pressures and heat fluxes.

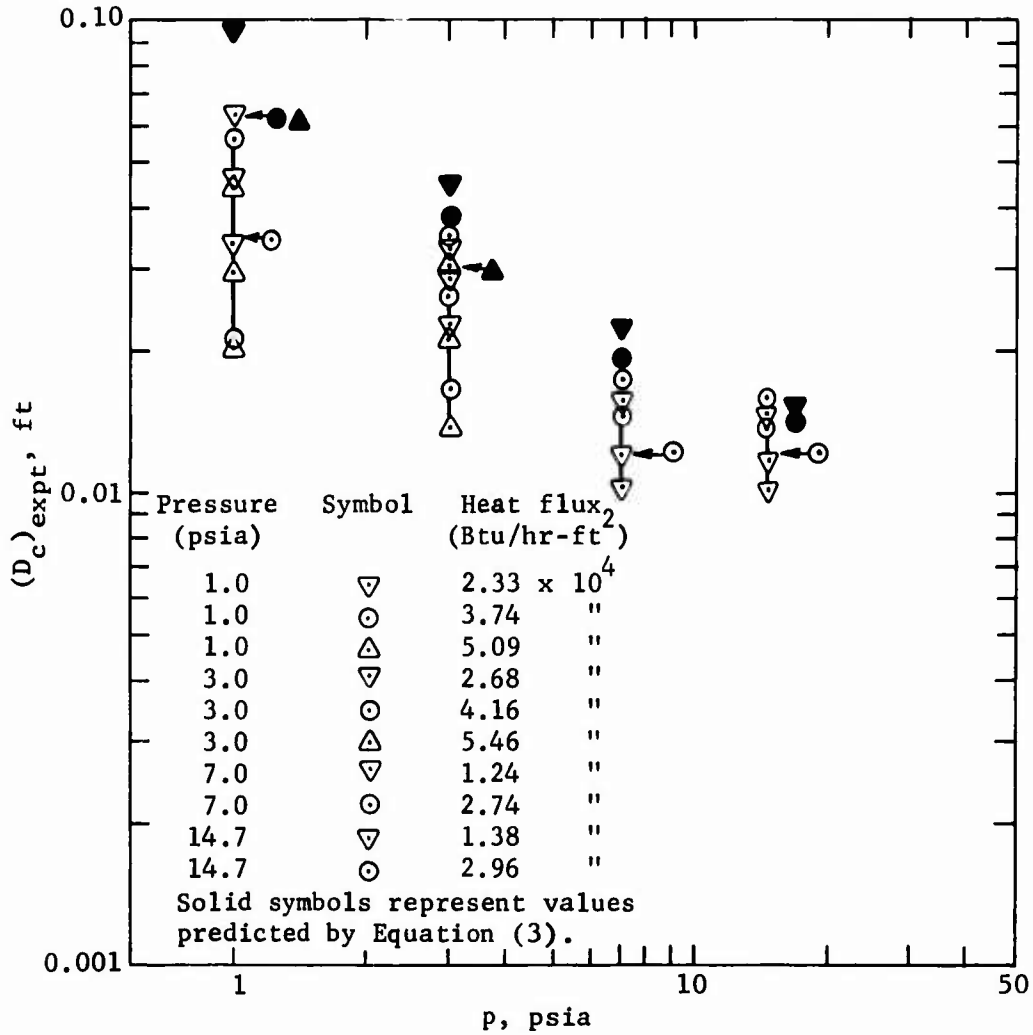

Fig. 10. Maximum, minimum and average values of bubble diameters at departure from 0.026-inch-diameter wire at various pressures and heat fluxes.

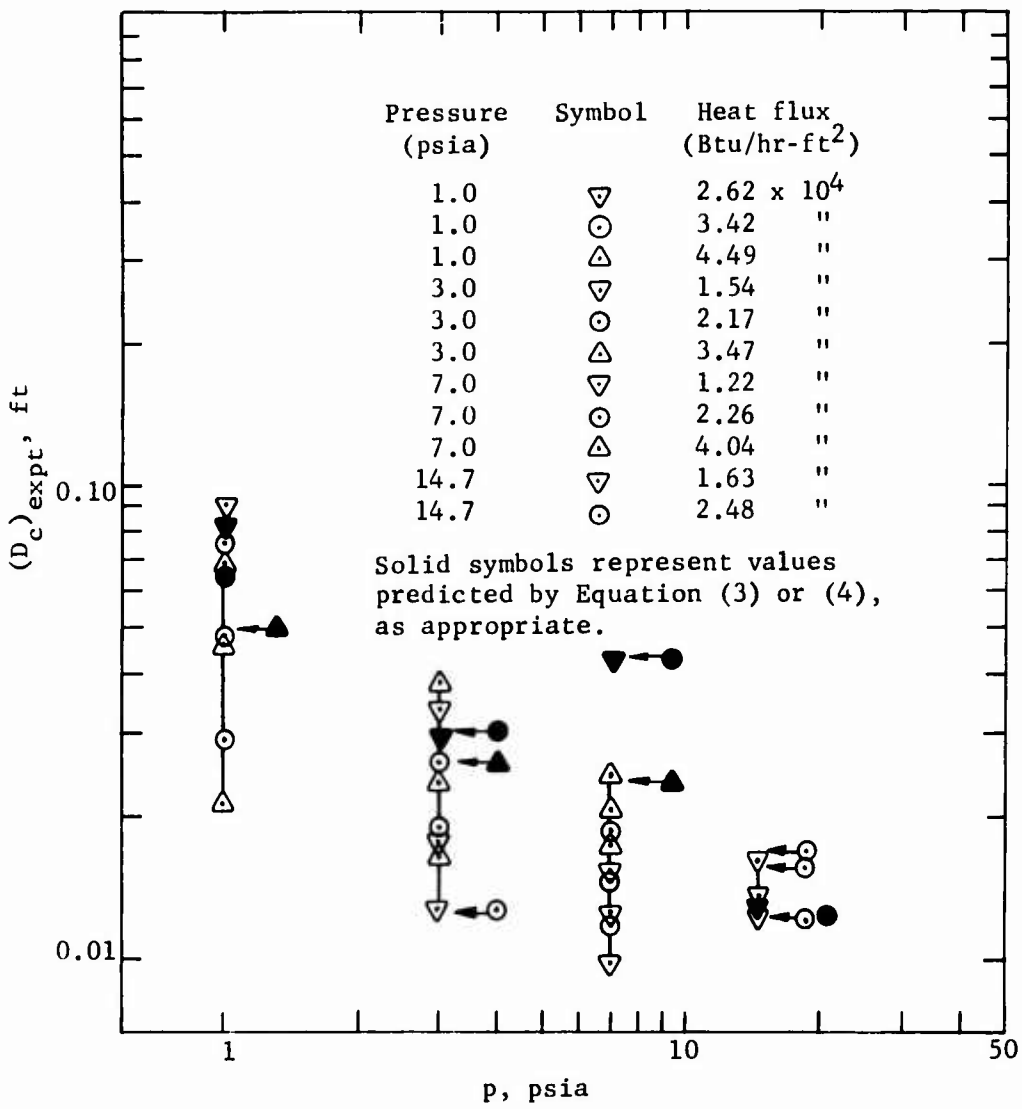

Fig. 11. Maximum, minimum and average values of bubble diameters at departure from 0.0506-inch-OD tube at various pressures and heat fluxes.

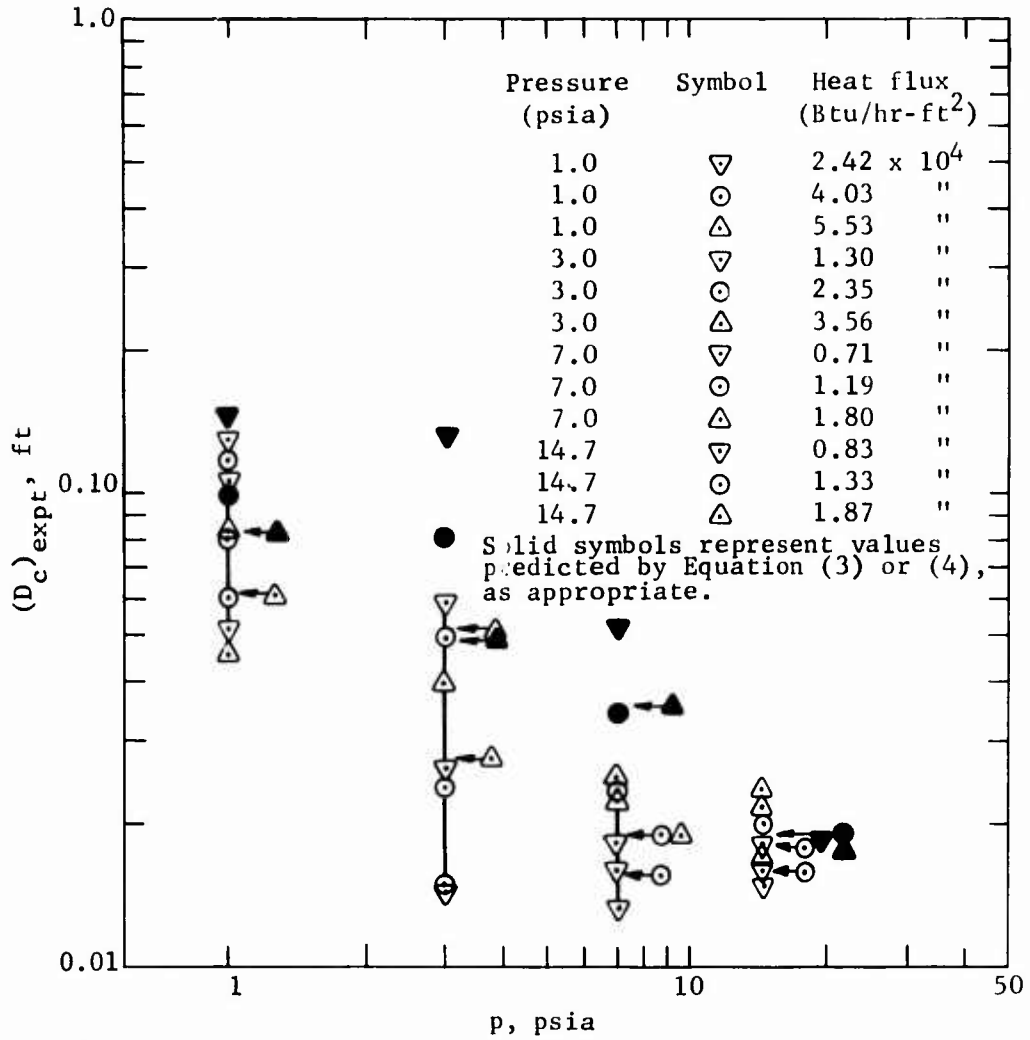

Fig. 12. Maximum, minimum and average values of bubble diameters at departure from 0.100-inch-OD tube at various pressures and heat fluxes.

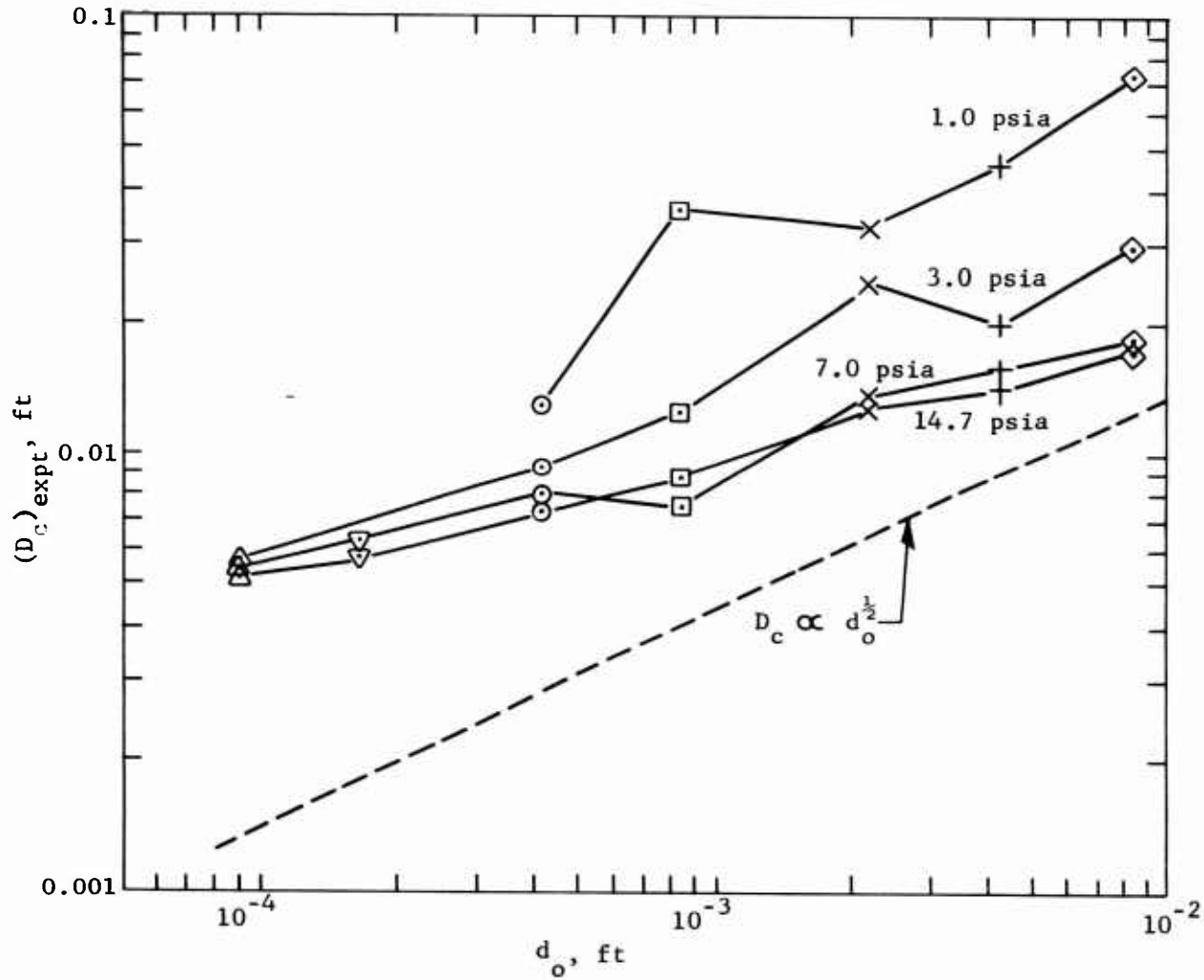

Fig. 13. Effect of heating surface diameter upon the average bubble diameter at departure in saturated nucleate pool boiling of water.

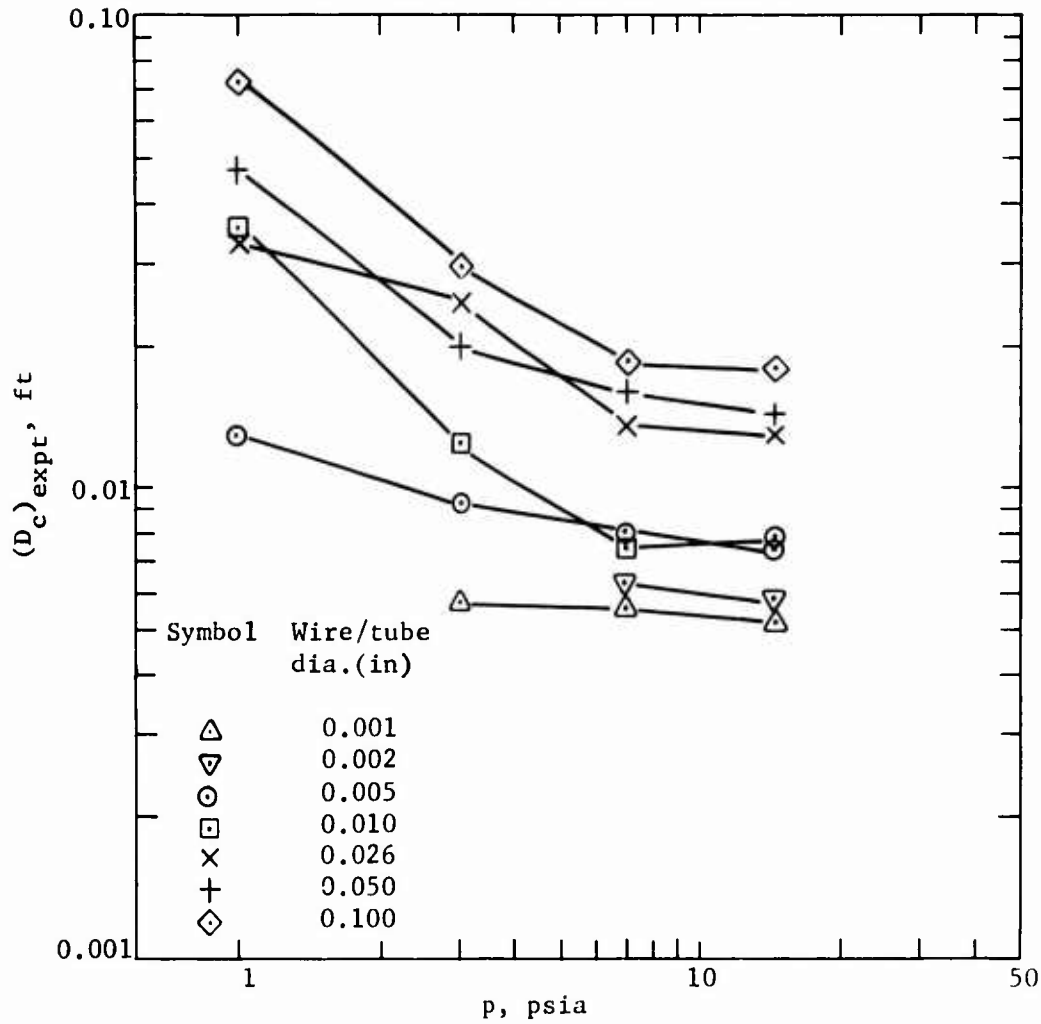

Fig. 14. Effect of pressure upon the average bubble diameter at departure in saturated nucleate pool boiling of water.

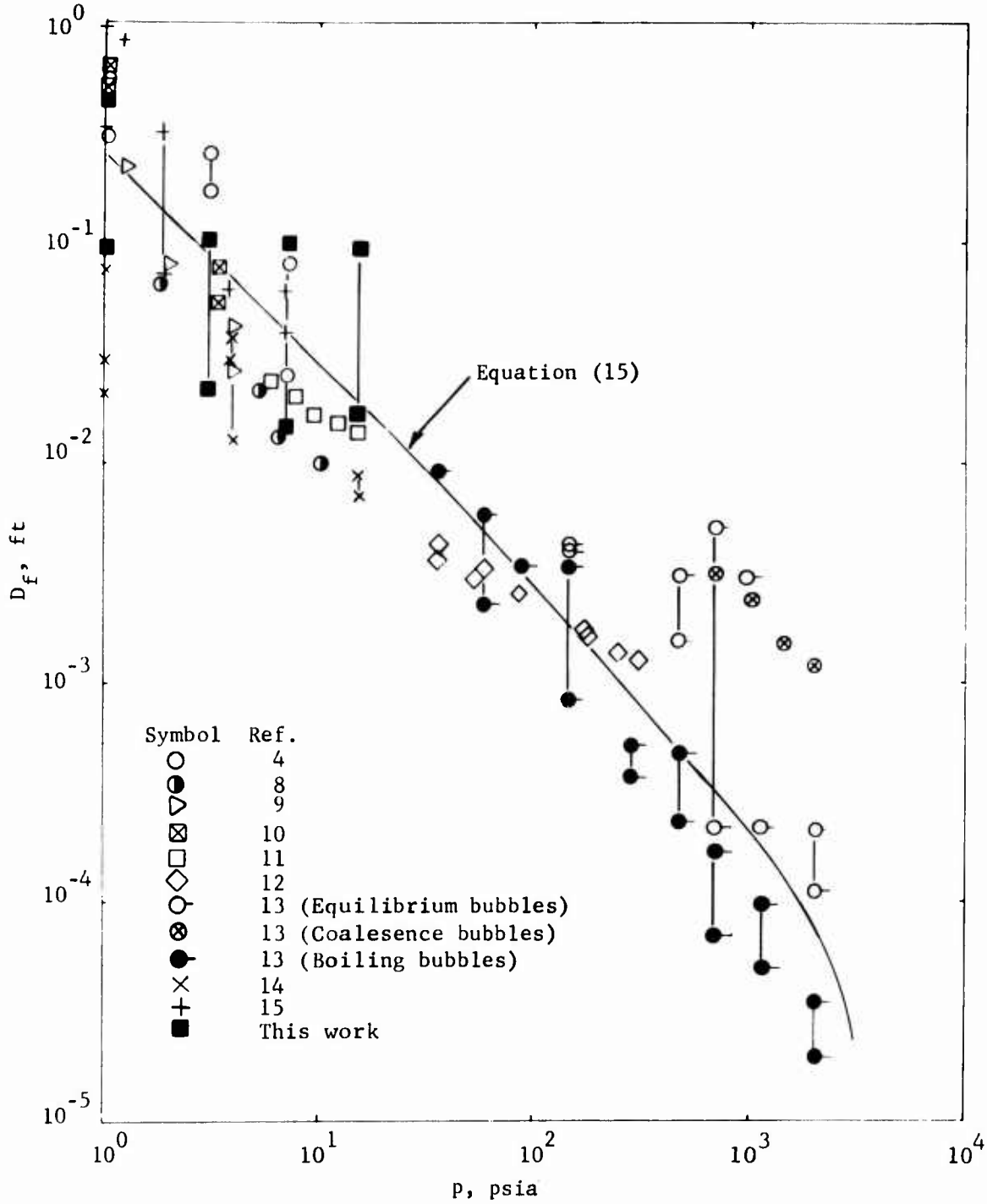

Fig. 15. Comparison of modified maximum bubble diameters with the correlation for nucleate pool boiling of saturated water.

APPENDIX A

MEASUREMENT OF DIAMETER OF THE VARIOUS HEATING ELEMENTS USED IN THE TEST PROGRAM

0.001-, 0.002- and 0.005-inch-nominal-diameter wires

The diameters of these wires were considered too small to be measured accurately either by a micrometer or by weighing known lengths using an accurate balance. The diameters of these wires were, therefore, determined using the resistivity method. The values of resistivity and temperature coefficient of resistivity were obtained from measurements carried out on the 0.02595-inch-diameter wire. The details of resistivity measurements are given in Appendix B. From these measurements, the diameters of the 0.001-, 0.002- and 0.005-inch-nominal-diameter wires were found to be 0.00107, 0.00201 and 0.00500 inch, respectively.

0.010- and 0.025-inch-nominal-diameter wires

The diameters of these wires were considered too small to be measured accurately by a micrometer. Since these wires were heavy enough to permit determination of their diameters by accurately weighing known lengths, this method was preferred over the less accurate resistivity method. The lengths and weights of approximately nine inch long samples were measured accurately. Assuming the density of platinum to be 1335 pounds per cubic foot, these diameters were calculated to be 0.01005 and 0.02595 inch, respectively.

0.05- and 0.10-inch-nominal-OD tubes

Accurate measurement of the outer diameters of the 0.05- and 0.10-inch-nominal-OD tubes was carried out using a micrometer capable of reading 0.0001 inch. Average OD of the two tubes was found to be 0.0506 and 0.1000 inch, respectively. The average inner diameter of these tubes was determined indirectly by accurately weighing known lengths, and found to be 0.03725 and 0.09116 inch, respectively.

APPENDIX B

MEASUREMENT OF RESISTIVITY AND TEMPERATURE COEFFICIENT OF RESISTIVITY OF THE VARIOUS WIRES AND TUBES

Approximately six inch lengths of various wires and tubes were mounted horizontally between current carrying conductors and the lengths measured accurately by a vernier caliber capable of measuring it to an accuracy of 0.001 inch. The assembly was lowered into a tank of demineralized water at room temperature and the wire or tube placed as resistance R_x in the circuit shown below.

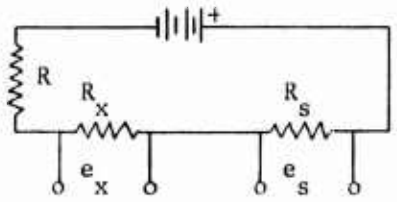

where R_s = standard resistance (ohm)

R = 200 Ω (approx.) for wires of nominal diameter between 0.001 and 0.010 inch

= 27 Ω (approx.) for wire of 0.025-inch nominal diameter and tubes of 0.05- and 0.10-inch nominal OD

R_x = resistance of the heating element under investigation at temperature T (ohm)

e_s, e_x = voltage drop across R_s and R_x, respectively (volt).

The resistance R was used simply to reduce the power input to resistances R_x and R_s. The temperature of water in the tank was maintained at either room temperature or at the boiling point at atmospheric pressure, and measured accurately in each case at the wire or tube level by a calibrated thermocouple.

During calibration of 0.001-, 0.002-, 0.005- and 0.010-inch-nominal-diameter wires, the emf from the dc source was adjusted to limit the current flow to between 20 and 25 milliamperes. Similarly, for the 0.025-inch-nominal-diameter wire and the 0.005- and 0.10-inch-nominal-OD tubes, the current flow was limited to between 140

and 190 milliamperes. At these low current levels, the temperature rise in the wires or tubes was limited to less than 0.1°F. After steady state conditions were reached, the values of e_s, e_x and water temperature were recorded.

For wires of nominal diameter 0.001, 0.002 and 0.005 inch, the accurate values of the diameter were obtained from:

$$d_o^2 = \frac{4\phi_{32}\ell e_s}{\pi R_s e_x}\left\{1 + \alpha(T_f - 32)\right\} \quad , \tag{B-1}$$

where d_o = outer diameter of the heating element (ft)

ϕ_{32} = resistivity of the heating element at 32°F (ohm-ft)

ℓ = length of the heating element (ft)

α = temperature coefficient of resistivity (F^{-1})

T_f = temperature of water (F) .

The values of ϕ_{32} and α for Equation (B-1) were obtained from tests carried out with the 0.02595-inch-diameter wire. These values were $\phi_{32} = 3.38 \times 10^{-7}$ (ohm-ft) and $\alpha = 0.0020$ (f^{-1}).

The resistivity and temperature coefficient of resistivity values for wires of 0.01005 and 0.02595 inch diameter were obtained by solving the simultaneous Equations (B-2) and (B-3), and those for the 0.0506- and 0.100-inch-OD tubes were obtained by solving Equations (B-4) and (B-5), shown below, all using measured values of e_s and e_x at two temperatures. For wires,

$$\left\{\frac{R_s e_x}{e_s}\right\}_{rt} = \frac{4\phi_{32}\ell}{\pi d_o^2}\left\{1 + \alpha(T_{frt} - 32)\right\} \quad , \tag{B-2}$$

$$\left\{\frac{R_s e_x}{e_s}\right\}_{ht} = \frac{4\phi_{32}\ell}{\pi d_o^2}\left\{1 + \alpha(T_{fht} - 32)\right\} \quad ; \tag{B-3}$$

for tubes,

$$\left\{\frac{R_s e_x}{e_s}\right\}_{rt} = \frac{4\phi_{32}\ell}{\pi(d_o^2-d_i^2)}\left\{1 + \alpha(T_{frt}-32)\right\} , \qquad \text{(B-4)}$$

$$\left\{\frac{R_s e_x}{e_s}\right\}_{ht} = \frac{4\phi_{32}\ell}{\pi(d_o^2-d_i^2)}\left\{1 + \alpha(T_{fht}-32)\right\} ; \qquad \text{(B-5)}$$

where d_i is the inner diameter of tube (ft), subscript rt is the value at room temperature, and subscript ht is the value when boiling at atmospheric pressure.

The following computed values were used in all subsequent calculations.

wire or tube OD (in)	ϕ_{32} (ohm-ft)	α ($^\circ F^{-1}$)
0.00107	3.38×10^{-7}	0.0020
0.00201	3.38 "	0.0020
0.00500	3.38 "	0.0020
0.01005	3.325 "	0.0020
0.02595	3.38 "	0.0020
0.0506	3.681 "	0.002016
0.1000	3.715 "	0.001874

APPENDIX C

DETERMINATION OF SURFACE TEMPERATURE OF THE HEATING ELEMENTS

In all tests reported here, the outer surface temperature of heating elements, T_w, was calculated from the measured values of the current flowing through and the voltage drop across them. Spot welding a thermocouple on the wire or tube surface was considered unsuitable for this investigation because, (a) spot welding a thermocouple would have significantly changed the characteristics of the location in boiling to make measurements unrepresentative of the entire surface, (b) the wire diameter and the tube wall thicknesses were small, (c) only a small surface area of the thermoucouple would have actually come in contact with the heating surface, the rest being in contact with the liquid, and (d) local wall temperature fluctuations caused by boiling would have made measurement of the average heating surface temperature very difficult. Instead, it was decided to determine the average wall temperature using the heating surface as a resistance heater, as described below.

For a given set of experimental conditions, the measured values of the current flowing through the heating element and the voltage drop across it gave the value of the total resistance of the heating element at its average or mean temperature. From this average temperature value, the outer surface temperature was calculated as follows.

Wires

Assuming the temperature to vary with radius only, the heat generated in a cylinder of radius r is conducted outwards, and may be written:

$$q''' \pi r^2 \ell = -2\pi r \ell K \frac{dT}{dr} \quad , \qquad \text{(C-1)}$$

where q''' is the heat generation rate in the heating element (Btu/hr-cu ft), K is the thermal conductivity of the heating element (Btu/hr-ft-F), and T is the temperature (F). If $T = T_c$ at $r = 0$, and $T = T_w$ at $r = r_o$, then Equation (C-1) may be integrated to give:

$$T_c - T_w = \frac{q''' r_o^2}{4K} \quad . \qquad \text{(C-2)}$$

For small diameter wires, the temperature drop from the center of the wire to outside is not large. Therefore, in this derivation, it was assumed that the effect of temperature coefficients of electrical resistivity and thermal conductivity upon the heat generation rate in the heating element was negligible. The heat generation rate in the wire may now be equated to the heat flux on its surface to give:

$$q'''\pi r_o^2 \ell = q 2\pi r_o \ell \quad , \tag{C-3}$$

or

$$q''' = \frac{2q}{r_o} \quad . \tag{C-4}$$

From Equations (C-2) and (C-4),

$$T_c - T_w = \frac{q r_o}{2K} \quad , \tag{C-5}$$

where $$q = \frac{3.413\ V\ I}{2\pi r_o \ell} \tag{C-6}$$

V = voltage drop across the heating element (volt)

I = current flowing through the heating element (amp).

To confirm the assumption of small temperature drop within the wire, temperature drop across the largest diameter wire used in these tests was calculated at the maximum experimental heat flux of 54,600 Btu/hr-sq ft, and found to be 0.7°F. Therefore, the assumption of constant heat generation rate was reasonable. The mean temperature of the wire may now be related to its outer wall temperature as follows. Assuming a linear temperature drop across the wire for small diameter wires, the wire temperature at any radius r may be written as:

$$T = T_w + \frac{r_o - r}{r_o} (T_c - T_w) \quad , \tag{C-7}$$

and the mean temperature of the wire may be written as:

$$T_m = \frac{\int_0^{r_o} 2\pi r dr \left\{T_w + \frac{r_o - r}{r_o}(T_c - T_w)\right\}}{\pi r_o^2}$$

$$= T_w + \frac{1}{3}(T_c - T_w) \quad . \qquad \text{(C-8)}$$

The mean temperature, T_m, is calculated from measured values of current, voltage drop, and length and diameter of the wire as:

$$T_m = 32 + \frac{\pi r_o^2 V - I\phi_{32}\ell}{\alpha I \phi_{32}\ell} \quad . \qquad \text{(C-9)}$$

From Equations (C-5), (C-6), (C-8) and (C-9), one obtains:

$$T_w = \frac{\pi r_o^2 V - I\phi_{32}\ell}{\alpha I \phi_{32}\ell} + 32 - \frac{3.413\ V\ I}{12\pi K \ell} \qquad \text{(C-10)}$$

The corrections in the value of T_w caused by the temperature coefficients of thermal conductivity and electrical resistivity were found to be negligible.

Tubes

Assuming linear variations in thermal conductivity and electrical resistivity with temperature, the temperature drop across the wall of a tube may be written[16] as:

$$T_i - T_w = \frac{q r_o (R_m/R_i)}{K_i \left\{(r_o/r_i)^2 - 1\right\}} \left[\left\{\frac{r_o - r_i}{r_i}\right\}^2 - \frac{1}{3}\left\{\frac{r_o - r_i}{r_i}\right\}^3 + \frac{1}{4}\left\{\frac{r_o - r_i}{r_i}\right\}^4 + \ldots \right.$$

$$\left. + \frac{q r_o (R_m/R_i)}{6K_i \left\{(r_o/r_i)^2 - 1\right\}} \left\{\frac{r_o - r_i}{r_i}\right\}^4 \left\{\frac{3\gamma + 4\alpha\gamma T_i + \alpha}{(1+\alpha T_i)(1+\gamma T_i)}\right\} + \ldots \right] \quad , \qquad \text{(C-11)}$$

where T_i = inner tube wall temperature (F)

r_i = inner tube radius (ft)

R_m = mean tube resistance (ohm)

R_i = tube resistance at the tube inner wall temperature (ohm)

K_i = thermal conductivity of the tube at inner tube wall temperature (Btu/hr-ft-F)

γ = temperature coefficient of thermal conductivity (F^{-1}).

Simplifying the geometric term, Equation (C-11) may be written as:

$$T_i - T_w = \frac{q\, r_o\, (R_m/R_i)}{K_i \left\{(r_o/r_i)^2 - 1\right\}} \left[\frac{1}{2}\left\{\frac{r_o - r_i}{r_i}\right\}^2 + \left\{\frac{r_o - r_i}{r_i}\right\} - \log_e (r_o/r_i)\right.$$

$$\left. + \frac{q\, r_o\, (R_m/R_i)}{6K_i \left\{(r_o/r_i)^2 - 1\right\}} \left\{\frac{r_o - r_i}{r_i}\right\}^4 \left\{\frac{3\gamma 4\alpha\gamma T_i + \alpha}{(1+\alpha T_i)\,(1+\gamma T_i)}\right\} + \ldots\right] \qquad \text{(C-12)}$$

To determine the influences of the temperature coefficients of electrical resistivity and thermal conductivity, the temperature drop across the tube wall may now be calculated for both tubes. For the 0.100-inch-OD tube at the highest value of heat flux of 55,250 Btu/hr-sq ft at 1.0 psia obtained in the test program, the temperature drop across the tube wall assuming $\alpha = 0$ and $\gamma = 0$ was found to be 0.25°F. Using values of $\alpha = 0.0020°F^{-1}$ and $\gamma = 0.0003°F^{-1}$, the correction term was found to be negligibly small. Similarly, the temperature drop across the wall of the 0.0506-inch-OD tube for the highest heat flux of 44,850 Btu/hr-sq ft at 1.0 psia was found to be 0.32°F, the correction term involving α and γ being negligible.

Since only the mean temperature of the tube wall was determined from resistance measurements, values of $(T_i - T_w)$ obtained from Equation (C-12) had to be modified. The mean temperature was related to the tube outer wall temperature as follows. Referring to the tube cross-section shown below, the temperature at any radius r is given by:

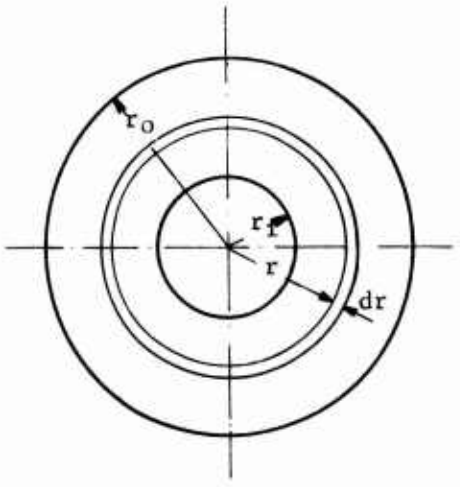

$$T = T_w + (T_i - T_w) \left\{ \frac{r_o - r}{r_o - r_i} \right\} , \qquad \text{(C-13)}$$

and the mean temperature of the tube, T_m, may be written as:

$$T_m = \frac{\int_{r_i}^{r_o} 2\pi r dr \left\{ T_w + (T_i - T_w) \left(\frac{r_o - r}{r_o - r_i} \right) \right\}}{\pi (r_o^2 - r_i^2)}$$

$$= T_w + (T_i - T_w) \left[\frac{r_o^2 + r_i r_o - 2 r_i^2}{3 (r_o^2 - r_i^2)} \right] . \qquad \text{(C-14)}$$

The values of the terms in the bracket for the 0.0506-inch-OD and 0.100-inch-OD tubes were found to be 0.47 and 0.49, respectively. Therefore, Equation (C-14) may be written as:

$$T_m = T_w + 0.47 (T_i - T_w) \text{ for the 0.0506-inch-OD tube} \qquad \text{(C-15)}$$

and

$$T_m = T_w + 0.49 (T_i - T_w) \text{ for the 0.1000-inch-OD tube .} \qquad \text{(C-16)}$$

Based upon the measured values of current flowing through and the voltage drop across a tube of length ℓ, the mean temperature may be written as:

$$T_m = 32 + \frac{\pi(r_o^2 - r_i^2)\, V - I\phi_{32}\ell}{\alpha I \phi_{32}\ell} \quad . \qquad \text{(C-17)}$$

Ignoring the correction term due to temperature coefficients of electrical resistivity and thermal conductivity and assuming $R_m = R_i$, Equation (C-12) gives:

$$T_i - T_w = 2.92 \times 10^{-4}\ q/K_i \text{ for the 0.0506-inch-OD tube} \qquad \text{(C-18)}$$

and

$$T_i - T_w = 1.86 \times 10^{-4}\ q/K_i \text{ for the 0.1000-inch-OD tube .} \qquad \text{(C-19)}$$

The outer wall temperature of the 0.0506-inch-OD tube may now be obtained by combining Equations (C-15), (C-17) and (C-18) to give:

$$T_w = 32 + \frac{\pi(r_o^2 - r_i^2)\, V - I\phi_{32}\ell}{\alpha I \phi_{32}\ell} - \frac{1.37 \times 10^{-4} q}{K_i} \quad , \qquad \text{(C-20)}$$

and for the 0.1000-inch-OD tube, Equations (C-16), (C-17) and (C-19) may be combined to give:

$$T_w = 32 + \frac{\pi(r_o^2 - r_i^2)\, V - I\phi_{32}\ell}{\alpha I \phi_{32}\ell} - \frac{9.11 \times 10^{-5} q}{K_i} \quad . \qquad \text{(C-21)}$$

For all data reported here, the surface temperature of wires was determined using Equation (C-10) and those of the 0.0506-inch- and 0.1000-inch-OD tubes using Equations (C-20) and (C-21), respectively.

REFERENCES

1. Naval Civil Engineering Laboratory. Technical Note N-1069: The effect of system parameters on the maximum bubble diameter in saturated nucleate boiling of liquids, by S. C. Garg. Port Hueneme, California, December 1969.

2. United Kingdom Atomic Energy Authority. Report no. AEEW-R-180: An analytical and experimental study of pool boiling with particular reference to additives, by W. L. Owens. Winfrith, Dorset, England, May 1963.

3. H. J. Ivey and D. J. Morris, "Critical heat flux of saturation and subcooled pool boiling of water at atmospheric pressure," Proceedings of the Third International Heat Transfer Conference, Chicago, August 1966, vol. III, pp. 129-142.

4. S. C. Garg. Studies of the heat exchange process associated with the nucleate pool boiling of a liquid, Ph.D. thesis, Department of Mechanical Engineering, University of Edinburgh, Edinburgh, Scotland, October 1963.

5. Central Electricity Generating Board. Report on Contract no. 46: Nucleate boiling heat transfer, by T. D. Patten and S. C. Garg. University of Edinburgh, Edinburgh, Scotland, December 1964.

6. W. Fritz, "Calculation of maximum volume of vapor bubbles," Physikalische Zeitschrift, vol. 36, 1935, pp. 379.

7. R. F. Gaertner and J. W. Westwater, "Population of active sites in nucleate boiling heat transfer," Chemical Engineering Progress, Symposium Series no. 30, vol. 56, 1960, pp. 39-48.

8. A. P. Hatton and I. S. Hall, "Photographic study of boiling on prepared surfaces," Proceedings of the Third International Heat Transfer Conference, vol. IV, August 1966, pp. 24-37.

9. R. Cole, "Bubble frequencies and departure volumes at subatmospheric pressures," AIChE Journal, vol. 13, 1967, pp. 779-783.

10. T. D. Patten, "Some characteristics of nucleate boiling of water at sub-atmospheric pressures," paper presented at Thermodynamics and Fluid Mechanics Convention, Cambridge, England, 1964. (paper no. 9.)

11. K. Nishikawa and K. Urakawa, "An experiment of nucleate boiling under reduced pressures," Memoirs of Faculty of Engineering, Kyushu University, Japan, vol. 19, no. 3, March 1960, pp. 139-147.

12. R. L. Semeria, "An experimental study of the characteristics of vapor bubbles," Proceedings of the Institute of Mechanical Engineers, Symposium on Two Phase Flow, London, 1962, pp. 57-65.

13. R. L. Semeria, "Caractéristiques des bulles de vapeur sur une paroi chauffente dans l'eau en ébullition à haute pression," Academie Des Sciences, Comptes Rendus, vol. 256, no. 6, February 4, 1963, pp. 1227-1230

14. I. A. Raben, R. I. Beaubouef and G. E. Commerford, "A study of heat transfer in nucleate pool boiling of water at low pressures," Chemical Engineering Progress, Symposium Series no. 57, vol. 61, 1965, pp. 249-257.

15. R. Cole and H. L. Shulman, "Bubble departure diameters at sub-atmospheric pressures," Chemical Engineering Progress, Symposium Series no. 64, vol. 62, 1966, pp. 6-16.

16. G. Leppert, C. P. Costello and B. M. Hoglund, "Boiling heat transfer to water containing a volatile additive," ASME Transactions, vol. 80, no. 7, October 1958, pp. 1395-1404.

NOMENCLATURE

A	Surface area of the heating element	ft^2
B_1	Ratio defined by Equation (7)	
B_2	Ratio defined by Equation (8)	
B_3	Ratio defined by Equation (9)	
C_1, C_2, C_3	Constants	
C_4	Dimensional Constant	
C_c	Constant for cylindrical heating surfaces which relates the thickness of the superheated layer in nucleate boiling where a bubble envelops the heating surface to its value assuming pure conduction, as defined by Equation (3)	
C_f	Constant which relates the thickness of the superheated layer in nucleate boiling to its value assuming pure conduction for flat surfaces and for cylindrical surfaces where the bubble diameter at departure is less than four times the diameter of the heating surface, as defined by Equation (4)	
C_ℓ	Specific heat of liquids	$Btu/lb_m\,^\circ F$
d_i	Inner diameter of tube	ft
d_o	Outer diameter of the heating element	ft
D_c	Bubble diameter at departure from a cylindrical heating surface	ft
D_e	Equivalent maximum bubble diameter at departure from a flat surface, as defined by Equation (5)	ft
D_f	Maximum bubble diameter at departure from a flat surface	ft

e_s	Voltage drop across resistance R_s during calibration	Volt
e_x	Voltage drop across resistance R_x during calibration	Volt
g	Earth acceleration	ft/hr^2
g_o	Conversion factor, $4{\cdot}18 \times 10^8$ ft/hr^2	$lb_m\text{-}ft/lb_f\text{-}hr^2$
h_{fg}	Latent heat of evaporation	Btu/lb_m
I	Current flowing through the heating element	amp
k	Thermal conductivity of liquid	Btu/hr-ft-F
K	Thermal conductivity of the heating element	Btu/hr-ft-F
K_i	Thermal conductivity of tube at the inner wall temperature	Btu/hr-ft-F
ℓ	Length of heating element	ft
p	System pressure	lb_f/in^2
p_c	Critical pressure	lb_f/in^2
q	Heat flux at the surface of the heating element	$Btu/hr\text{-}ft^2$
q'''	Heat generation rate in the heating element	$Btu/hr\text{-}ft^3$
r	Radius	ft
r_i	Inner radius of tube	ft
r_o	Outer radius of the heating element	ft
R	Electrical resistance	ohm
R_i	Electrical resistance of the tube at inner wall temperature	ohm

R_m	Electrical resistance of the tube at mean temperature	ohm
R_s	Standard electrical resistance used during calibration	ohm
R_x	Electrical resistance of the heating element during calibration	ohm
T	Temperature of the heating element at any location	F
T_c	Temperature at the center of wire	F
T_f	Temperature of water during calibration	F
T_i	Inner tube wall temperature	F
T_m	Mean temperature of the heating element	F
T_s	Saturation temperature of water	F
T_w	Outer surface temperature of the heating element	F
ΔT	Wall to saturation temperature difference	F
V	Voltage drop across the heating element	Volt
α	Temperature coefficient of electrical resistivity	F^{-1}
γ	Temperature coefficient of thermal conductivity	F^{-1}
ϕ_{32}	Resistivity of the heating element at 32°F	ohm-ft
ρ_ℓ	Density of liquid	lb_m/ft^3
ρ_v	Density of vapor	lb_m/ft^3
σ	Surface tension	lb_f/ft

Subscripts

rt	During the room temperature calibration test
ht	During boiling at atmospheric pressure calibration test
expt	Experimental value
pred	Predicted value

ZFXX-112-001

AD-864 688
TAB 70-7

AD-876 732 mbb
Tab 70-1

Naval Ordnance Lab., White Oak, Silver Spring, Md.